Optimum reinforcement design of a passenger vehicle door panel to minimise vibrational deformation

Jinoh Yang

Jinoh Yang

Supervised by Dr. Jon Trevelyan and Prof. Peter Bettess

A Thesis for the Degree of Master of Science

Optimum Reinforcement Design of a Passenger Vehicle Door Panel to Minimise Vibrational Deformation

by

Jinoh Yang

A Thesis submitted in partial fulfilment
of the requirements for the degree of
Master of Science

School of Engineering
The University of Durham
1998

Contents

Acknowledgements

It was a great fortune and a glory for me to study in Durham which is a historical, academic and religious city. I am very proud of having studied my MSc research in Durham University. The past one year will be the most meaningful and thankful term in my whole life.

I appreciate my supervisors Dr. Jon Trevelyan and Prof. Bettess who have helped me with my research. My dissertation could not have been completed without their help.

I appreciate Hyundai Motor Company for supporting my research and life in England financially. I only hope that my research become to be helpful to car body design.

Also I appreciate Dr. Dominy who kindly gave me air pressure data for a driven car.

I thank deeply my family and brothers in God for praying for me always.

And lastly I thank to my colleagues who send the CAD data willingly to me for my study.

Above all I appreciate God Who gave me a chance to study in Great Britain and completed His plan.

Nomenclature

C_p Pressure coefficient, $C_p = \frac{p - p_\infty}{\frac{1}{2}\rho U^2}$

c Viscous damping coefficient

c_c Critical viscous damping coefficient

D Bending stiffness

d Characteristic dimension

E Young's modulus

e Volumetric strain

F External force

f Frequency (Hz)

G Shear elasticity modulus

I Second moment of area

k Stiffness

L Vehicle length

M Bending moment

m Mass

p Local static pressure

p_∞ Free-stream static pressure

Q Shear force

r Frequency ratio, $r = \frac{\omega}{\omega_n}$

Re Reynolds number, $Re = \frac{\rho \upsilon L}{\mu}$

T Natural period of vibration, $T = 1/f$

x, ϕ Displacement

α Phase angle

δ Logarithmic decrement

ε Normal strain

γ Shear strain

λ Eigenvalue

μ Viscosity coefficient of fluid

ν Poisson ratio, $\nu = \left| \frac{\text{lateral strain}}{\text{axial strain}} \right|$

ρ Density of materials

σ Normal stress

τ Shear stress

υ Vehicle velocity

ω Forced frequency (rad/sec)

ω_d Damped natural frequency (rad/sec)

ω_n Undamped natural frequency (rad/sec)

ω_{od} Overdamped natural frequency (rad/sec)

ζ Viscous damping ratio, $\zeta = \frac{c}{c_c}$

List of Figures

Abstract

Full-scale wind tunnel experiments and analysis using CFD (Computational Fluid Dynamics) are already developed and applied to the research and development processes of current passenger vehicles.[1] But from the viewpoint of the indoor aspiration noise during high speed driving, the vibration of a passenger vehicle's door frame is a major influence. The vibrational deformation gives rise to aspiration noise, which is airborne sound transmitted through the gap between the door panel frame and the sealing system mounted on the body panel. The optimised design of a passenger vehicle's door frame can lead us to the minimisation of aspiration noise. The optimisation is carried out by the finite element analysis of the vibration of the passenger vehicle's door panel assembly under steady-state sinusoidal dynamic air pressure. The commercial analysis package ABAQUS[5-9] is applied to all analyses in this thesis.

The thesis concludes with recommendations for door reinforcement configurations to reduce aspiration wind noise, but such an optimum must be considered in relation to the associated financial costs and weight penalties.

1. Introduction

The process of modern vehicle design and manufacturing techniques causes engineers to consider not only the basic performance but also the safety and convenience for drivers and passengers. So improvements of the strength and stiffness of a vehicle structure and the installation of front or side air bags are provided against any kind of collision and its effects. In addition, any noise on driving (for example, engine noise, body vibrating noise, friction noise between inside trims, and wind noise) is now considered to be an important factor in the assessment of a vehicle's performance. In particular, wind noise has become a primary factor by which we can assess the quality and convenience when a vehicle is driven at a high speed. The powertrain noise has been more important in the past, but developments in the quality of automobiles have been made to reduce the powertrain noise substantially. This results in the comparative importance of wind noise as a contributor to the total noise.

An optimisation for impact may suggest a different design. In a design to resist side impact, the side impact safety bar and pad located in the below door belt region and the reinforcement of the B-pillar lower part are the traditional solutions in the body panel part. But the most important concept of the side impact safety in the body panel part is to make the door panel and the side structure more absorptive against the impact, and more stiff as well.

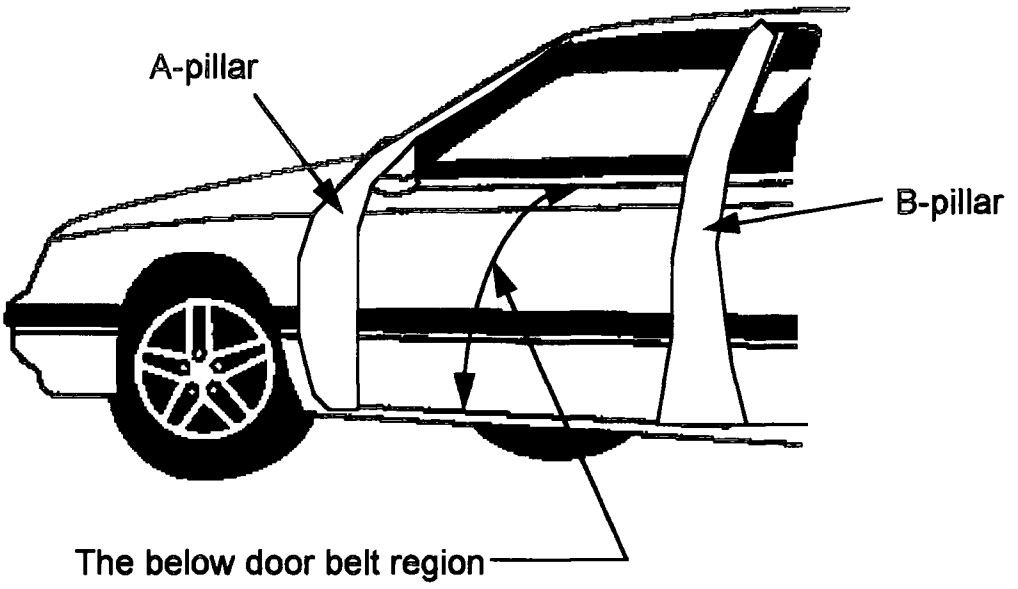

Figure 1-1. A, B-pillar and the below door belt region of a vehicle

Full-scale wind tunnel experiments and analysis using CFD are already developed and applied to the research and development processes of actual passenger vehicles.[1] But from a viewpoint of indoor aspiration noise (which is defined as sound transmitted through the gap between the door panel frame and the sealing system mounted on the body panel) when a vehicle is driven at high speed, the vibration of a passenger vehicle's door frame becomes one of the primary factors.[2-3] At high speed, the door frame vibrates because of the pressure difference between the air inside and outside the passenger compartment. Therefore if the door frame is optimally designed to prevent vibrational deformation over the appropriate frequency range, the aspiration noise should be reduced. Adding reinforcements to the door frame region makes the door panel more resistant to bending deformation, but in

proportion to the addition of the reinforcement, the weight and the cost of the vehicle are increased. Therefore the optimisation to balance the addition of the reinforcement against the weight and the cost of the vehicle is very commercially significant.

The optimisation may be carried out by the analysis of the vibration modes of the passenger vehicle's door panel assembly. A computational analysis, such as that used in this research, not only saves time but also money in the step of prototype development. Finite element analysis provides a much more quick and cheap method of assessment than prototype tests or full-scale wind tunnel test. By use of such a computer system an engineer can modify possible solutions and find an appropriate final solution.

The finite element method is a numerical procedure for the solution of differential equations. The major concept of the finite element method is that any continuous quantity, such as temperature, pressure, or displacement, may be approximated as a discrete model composed of a group of a piecewise continuous functions which are defined over a finite number of subdomains.[4] The modelling and analysis are performed using commercial package ABAQUS[5-9].

2. Vehicle Door Design

2.1. General Concept of Vehicle Door Design

Vehicle door design has many aspects for consideration by the engineer[10] :

- side impact safety (in order to improve the safety of driver or passenger from the side impact, some sub-materials are used such as anti-impact bars and impact absorbing pads)
- door frame stiffness
- wind noise
- opening-closing performance and endurance
- outside panel dent
- side door strength
- door glass up-down durability which is related to the window regulator and glass run system
- temperature resistance
- sagging which is very related to hinge and hinge face panel stiffness are the items should be considered.

In addition, the manufacturability is the most important part of vehicle door design.

- The formability of panels in the press process
- the possibility of tooling or assembly

- hemming possibility
- whether it is weldable or not
- paint drain capability in the painting process
- and cost, weight, process reduction are all fundamental to manufacturability.

In addition to the above, there are more details in the vehicle door design, such as

- the door opening system including inside, outside handle and latch,
- door checker which controls the door opening angle,
- door trims,
- many sorts of electric switches, for example, the power window switches or outside mirror control switches,
- the door sealing system usually made of rubber,
- the corrosion problem,
- and the opening gap and parting gap between the door and the side structure in the completed vehicle condition.

Each of these is very important to make the whole vehicle door.

2.2. Typical Design Process of Vehicle Door

A typical vehicle door design process is as follows :

1) Fix of exterior style line.
2) Sample car inspection and advanced study.
3) Door type determination, for example, full door, frame door, hidden frame door, or frameless door. The difference between a full door and a frame door is that a full door does not have a separate frame part, but a frame door does. In a hidden frame door the frame is hidden by a sealing system or the side window glass. When a door does not have a door frame in the window region, the door is called a frameless door.
4) Deciding whether new technology will be applied or not. If a new technology will be applied, all processes which are related to manufacturability, patent and law should be considered in advance.
5) Door opening gap check and parting gap decision. The opening gap is very important in every moving part. This must be checked in the step of exterior design.
6) Determination of the window regulator type and the regulating trace.
7) Determination of the sealing system. This is related to decide the door type.
8) Door panel assembly and the interior trims design using CAD, this includes the following :
    - Side impact safety such as anti-impact bar, absorbing pad, etc.
    - The passenger car door system crush test procedure as recommended by SAE J367 JUN80.[11]
    - Manufacturing processes such as press, welding, hemming, paint drain, etc.

- The strength and stiffness of the door panel assembly.
- Cost, weight, and process reduction.
- The durability of the door glass up-down and the door opening-closing system. SAE J934a[12] shows the passenger vehicle door hinge systems, and the passenger car side door latch systems are shown on SAE J839b[13].
- The convenience of assembly and installation.

9) Prototype door making.

10) Test of door assembly under all possible conditions[10]. Finite element analyses are carried out in parallel with actual vehicle experiments.

11) Continuous changes and improvements.

12) Re-test.

13) Pilot product entrance.

14) Re-test.

15) Final revision of drawing.

16) Mass production in-line.

In this thesis, it is assumed that wind noise increases with vibration amplitude, so the relationship between the air pressure and the vibrational deformation of the door panel is mainly considered. The SAE standard test procedure for sound level for passenger cars is presented in SAE J986b[14], and SAE J1030[15] recommends the maximum sound level for passenger cars.

3. Theories

3.1. Bending Theory of Thin Plate

In one-dimensional system under Hooke's Law, the normal stress σ and the normal strain ε are expressed by[16]

$$\varepsilon = \frac{\sigma}{E} \tag{3.1.1}$$

where E is Young's modulus.

Likewise, the shear stress τ and the shear strain γ may be given by

$$\gamma = \frac{\tau}{G} \tag{3.1.2}$$

where G is the shear elasticity modulus.

The relationship between Young's modulus E and the shear elasticity modulus G is presented by

$$G = \frac{E}{2(1+\nu)} \tag{3.1.3}$$

where ν is Poisson ratio which is shown as

$$\nu = \left| \frac{\text{lateral strain}}{\text{axial strain}} \right| \tag{3.1.4}$$

The shear elasticity modulus can be measured from torsion test, and Poisson ratio is obtained by using equation (3.1.3).

Extending equation (3.1.1) to general case, Hooke's Law may be written as

$$\varepsilon_x = \frac{1}{E}\left(\sigma_x - \nu\left(\sigma_y + \sigma_z\right)\right)$$

$$\varepsilon_y = \frac{1}{E}\left(\sigma_y - \nu(\sigma_x + \sigma_z)\right) \tag{3.1.5}$$

$$\varepsilon_z = \frac{1}{E}\left(\sigma_z - \nu(\sigma_x + \sigma_y)\right)$$

Likewise, the general expression of equation (3.1.2) using (3.1.3) may be written as

$$\gamma_{xy} = \frac{2(1+\nu)}{E}\tau_{xy}$$

$$\gamma_{yz} = \frac{2(1+\nu)}{E}\tau_{yz} \tag{3.1.6}$$

$$\gamma_{zx} = \frac{2(1+\nu)}{E}\tau_{zx}$$

Equation (3.1.5) and (3.1.6) can also be written as follows,

$$\sigma_x = \frac{\nu E}{(1+\nu)(1-2\nu)}e + \frac{E}{1+\nu}\varepsilon_x$$

$$\sigma_y = \frac{\nu E}{(1+\nu)(1-2\nu)}e + \frac{E}{1+\nu}\varepsilon_y \tag{3.1.7}$$

$$\sigma_z = \frac{\nu E}{(1+\nu)(1-2\nu)}e + \frac{E}{1+\nu}\varepsilon_z$$

$$\tau_{xy} = G\gamma_{xy} = \frac{E}{2(1+\nu)}\gamma_{xy}$$

$$\tau_{yz} = G\gamma_{yz} = \frac{E}{2(1+\nu)}\gamma_{yz} \tag{3.1.8}$$

$$\tau_{zx} = G\gamma_{zx} = \frac{E}{2(1+\nu)}\gamma_{zx}$$

where

$$e = \varepsilon_x + \varepsilon_y + \varepsilon_z \tag{3.1.9}$$

which is called volumetric strain.

Considering the plane stress system, stresses σ_z, τ_{yz}, and τ_{zx} are deleted, i.e.

$$\sigma_z = \tau_{yz} = \tau_{zx} = 0 \tag{3.1.10}$$

Thus equation (3.1.5) becomes

$$\varepsilon_x = \frac{1}{E}\left(\sigma_x - \nu\sigma_y\right)$$

$$\varepsilon_y = \frac{1}{E}\left(\sigma_y - \nu\sigma_x\right) \tag{3.1.11}$$

$$\varepsilon_z = -\frac{\nu}{E}\left(\sigma_x + \sigma_y\right)$$

Solving equation (3.1.11) for stresses gives

$$\sigma_x = \frac{E}{1-\nu^2}\left(\varepsilon_x + \nu\varepsilon_y\right) \tag{3.1.12a}$$

$$\sigma_y = \frac{E}{1-\nu^2}\left(\varepsilon_y + \nu\varepsilon_x\right) \tag{3.1.12b}$$

Figure 3-1 shows an infinitesimal element of a plate or shell which is under bending condition.[17] Note that this "element" should not be confused with a "finite element". The bending moments per unit length $M_x + \frac{\partial M_x}{\partial x}dx$ and $M_y + \frac{\partial M_y}{\partial y}dy$, the torsion moments per unit length $M_{xy} + \frac{\partial M_{xy}}{\partial x}dx$ and

$M_{yx} + \frac{\partial M_{yx}}{\partial y} dy$, and the shear forces per unit length $Q_x + \frac{\partial Q_x}{\partial x} dx$ and $Q_y + \frac{\partial Q_y}{\partial y} dy$ are applied to the shown surface of the element.

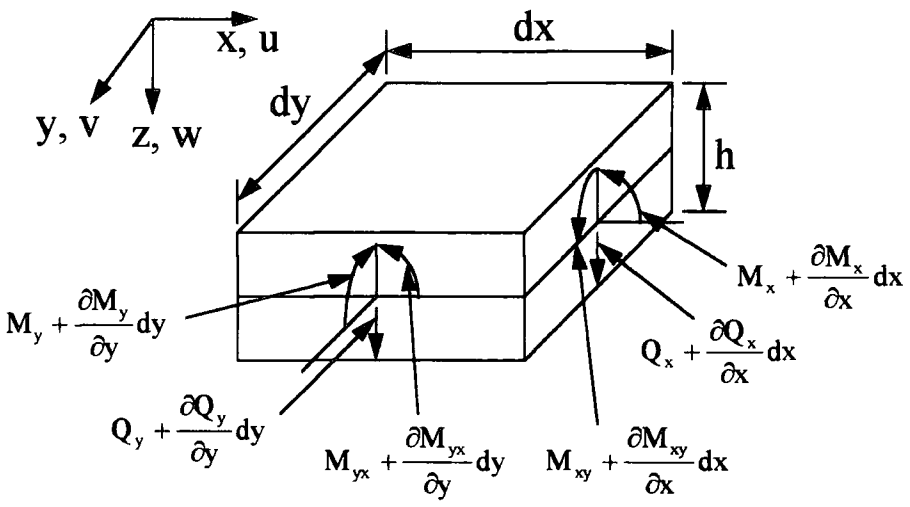

Figure 3-1. An infinitesimal element of a thin plate under bending

Symbols u, v, w are defined as displacements in each direction x, y, z.

The bending moments and the torsion moments per unit length may be obtained by integrating the appropriate stresses over the thickness-direction (z-direction).

$$M_x = \int_{-h/2}^{h/2} \sigma_x z dz = \frac{E}{1-\nu^2} \int_{-h/2}^{h/2} (\varepsilon_x + \nu \varepsilon_y) z dz$$

$$M_y = \int_{-h/2}^{h/2} \sigma_y z dz = \frac{E}{1-\nu^2} \int_{-h/2}^{h/2} (\varepsilon_y + \nu \varepsilon_x) z dz \qquad (3.1.13)$$

$$M_{xy} = -M_{yx} = -\int_{-h/2}^{h/2} \tau_{xy} z dz = \frac{-E}{2(1+\nu)} \int_{-h/2}^{h/2} \gamma_{xy} z dz$$

where h/2 is half the plate thickness, and z is the distance from the neutral surface.

The bending stresses which are located at distance z from the neutral surface may be written as

$$\sigma_x = \frac{M_x z dy}{I_y} = \frac{12M_x z}{h^3}$$

$$\sigma_y = \frac{M_y z dx}{I_x} = \frac{12M_y z}{h^3} \qquad (3.1.14)$$

$$\tau_{xy} = \tau_{yx} = \frac{12M_{xy} z}{h^3}$$

where I_x and I_y are second moments of area.

The strains which change linearly along the thickness-direction may be given by

$$\varepsilon_x = -z\frac{\partial^2 w}{\partial x^2}$$

$$\varepsilon_y = -z\frac{\partial^2 w}{\partial y^2} \qquad (3.1.15)$$

$$\gamma_{xy} = -2z\frac{\partial^2 w}{\partial x \partial y}$$

Substituting equation (3.1.15) into equation (3.1.13), the moments can be expressed as

$$M_x = -D\left(\frac{\partial^2 w}{\partial x^2} + \nu\frac{\partial^2 w}{\partial y^2}\right)$$

$$M_y = -D\left(\frac{\partial^2 w}{\partial y^2} + \nu\frac{\partial^2 w}{\partial x^2}\right) \tag{3.1.16}$$

$$M_{xy} = -M_{yx} = D(1-\nu)\left(\frac{\partial^2 w}{\partial x \partial y}\right)$$

where D is the bending stiffness written by

$$D = \frac{Eh^3}{12(1-\nu^2)} \tag{3.1.17}$$

and h is the thickness of the infinitesimal element.

Assuming a distributed load pdxdy is applied to the top surface of the element, the differential equations of the shear forces, bending and torsion moments may be written as

$$\frac{\partial Q_x}{\partial x} + \frac{\partial Q_y}{\partial y} + p = 0 \tag{3.1.18a}$$

$$\frac{\partial M_{xy}}{\partial x} - \frac{\partial M_y}{\partial y} + Q_y = 0 \tag{3.1.18b}$$

$$\frac{\partial M_{yx}}{\partial y} + \frac{\partial M_x}{\partial x} - Q_x = 0 \tag{3.1.18c}$$

From equations (3.1.18b) and (3.1.18c), substituting Q_x and Q_y to equation (3.1.18a)

$$\frac{\partial^2 M_x}{\partial x^2} - 2\frac{\partial^2 M_{xy}}{\partial x \partial y} + \frac{\partial^2 M_y}{\partial y^2} = -p \tag{3.1.19}$$

Substituting equation (3.1.16) to equation (3.1.19), the fourth order differential equation about a thin plate or shell shown as equation (3.1.20) is obtained.

$$\frac{\partial^4 w}{\partial x^4} + 2\frac{\partial^4 w}{\partial x^2 \partial y^2} + \frac{\partial^4 w}{\partial y^4} = \frac{p}{D} \qquad (3.1.20)$$

3.2. Fundamental Vehicle Aerodynamics

In aerodynamics, the researchers consider in terms of what happens when air flows past a stationary vehicle, instead of the real situation where the vehicle moves through the air. This is done because, in general, this is much easier to understand and describe the behaviour of the air flow than the actual condition.

When a vehicle is placed in a wind-tunnel, the relative speed of the air stream which is away from local changes caused by the presence of the vehicle is referred to as the free-stream speed. For the simple case of a vehicle driving in windless conditions, the corresponding relative speed is simply the driving speed of the vehicle.

The relationship between vehicle velocity υ and local static pressure (such as air pressure) p under aerodynamic conditions is given in the Bernoulli equation, which may be stated[1]

$$p + \frac{1}{2}\rho\upsilon^2 = \text{Constant} \qquad (3.2.1)$$

where ρ is the air density.

The air density ρ is 1.226kg/m^3 at the standard atmospheric sea-level.[18]

In equation (3.2.1), the term $\frac{1}{2}\rho\upsilon^2$ means the dynamic pressure caused by the moving vehicle.

The difference between the local static pressure at any point in a flow and the static pressure in the free stream depends on the dynamic pressure of the free stream.

The pressure coefficient C_p shows the above relationship by

$$C_p = \frac{p - p_\infty}{\frac{1}{2}\rho\upsilon^2} \qquad (3.2.2)$$

where p_∞ is the free-stream static pressure.

To describe the pressure variation around a vehicle, it is much more convenient to use the pressure coefficient rather than the actual pressure. Knowing the value of the pressure coefficient at a point, it is simple to calculate the value of the actual pressure at any driving speed, using equation (3.2.2).

When a car is driven, the behaviour of the boundary layer is greatly influenced by the pressure variation along the direction of flow. Other important factors are the speed, the density and viscosity of the air, and the geometric shape of the car.

The dependence of the flow patterns on speed, density, viscosity and length can be expressed by the Reynolds number Re as follows,

$$Re = \frac{\rho \upsilon L}{\mu} \tag{3.2.3}$$

where L is the vehicle length and μ is the air viscosity coefficient.

The standard sea-level air viscosity coefficient is 1.78×10^{-5} kg/m·sec.[18]

For fixed values of air density and viscosity, the Reynolds number is effectively dependent on the vehicle size and speed only.

If the Reynolds number is increased by increasing the speed of the vehicle, the flow transition position from laminar to turbulent moves forward, and the boundary layer becomes thinner. It can be seen that the value of the Reynolds number is important in determining the type of flow around the vehicle.

Consider an infinitely long circular cylinder of diameter d, which is under a vortex shedding condition. Each time a vortex is shed from the cylinder, the pressure distribution around the cylinder is disturbed. The shedding of vortices alternately from the two sides of the cylinder produces alternating lateral forces. As a result, these lateral forces cause a forced vibration of the cylinder at the same frequency as the frequency of vortex shedding.

Massey[19] shows the relationship between the frequency of vortex shedding and the vehicle speed using the Reynolds number in the following empirical formula,

$$\frac{f \cdot d}{\upsilon} = 0.198\left(1 - \frac{19.7}{Re}\right) \tag{3.2.4}$$

where f is the frequency of vortex shedding in cycles per second (hertz, Hz) and d is the characteristic dimension.

In equation (3.2.4), the quantity $\frac{f \cdot d}{\upsilon}$ is called the Strouhal number, after the Czech physicist Vincenz Strouhal who first investigated the 'singing' of wires in 1878.[1]

During normal driving condition, the Reynolds number is much larger than the value 19.7, so the value of $\frac{19.7}{Re}$ in equation (3.2.4) is near to zero. Therefore the formula can be written as,

$$\frac{f \cdot d}{\upsilon} \approx 0.198 \qquad (3.2.5)$$

The value of C_p which is applied to this thesis is from Howell[20], who investigated the side load distribution on a Rover 825i in a full-scale wind tunnel named MIRA, which has a cross section of 34.9m²(width 7.9m, height 4.4m) and is 15.2m long, under cross wind conditions when the wind speed is 100km/hr (28m/sec). It is the major concept of Howell's experiment that the pressure distribution over a vehicle surface under windy conditions is ruled by the aerodynamic yawing moment.

The principal dimensions of Rover 825i are : length 4.67m, width excluding mirrors 1.73m, height 1.40m, frontal area 2.03m², and no spoiler. This is similar in dimension to the Hyundai car which is the subject of this study, and therefore the pressure coefficients from Howell are used in this work.

C_p=0.5 is chosen for the pressure distribution in this research. Although in the below door belt region C_p has a different value, a typical value of C_p = 0.5 is found on the window glass part and this is chosen to simplify the pressure boundary condition. This is reasonable since the pressure in the glass region is dominant is calculating the door frame deformation in the vibrational modes of interest.

These data are supported by Docton[21-22] who studied vehicle behaviour under cross wind conditions.

The magnitude of the steady-state dynamic air pressure which is applied to the models may be calculated from equations (3.2.2), thus the value is 0.2363 Pa ($kg/m \cdot sec^2$) for the speed 100km/hr as considered by Howell.

3.3. Vibration

When a car is driven, a pressure difference arises between the inside and outside. The pressure difference is oscillatory at frequency 'f' defined in equation (3.2.4), and this gives rise to forced vibration of the structural panels of the vehicle.

All structures have their own natural frequencies, and according to the number of Degrees of Freedom (D.O.F) used to describe the mathematical model, a number of natural frequencies may be determined.

3.3.1. SDOF Vibration System

Figure 3-2 shows a single degree of freedom system which is under forced and damped vibration.[23-25]

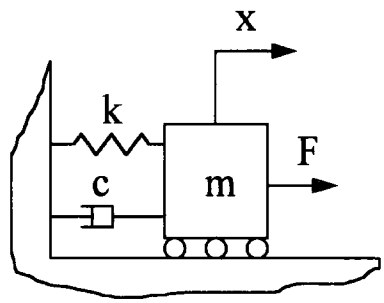

Figure 3-2. SDOF forced and damped vibration system

This system may be defined by a differential equation of motion as follows,

$$m\ddot{x}(t) + c\dot{x}(t) + kx(t) = F(t) \qquad (3.3.1)$$

where m is the mass of the system,

c is the viscous damping coefficient of the system,

k is the stiffness of the system,

$\ddot{x}$ is the acceleration of the system,

$\dot{x}$ is the velocity of the system,

x is the displacement of the system,

and F is the external force which is loaded to the system.

3.3.1.1. Free vibration system

If F(t) = 0 in equation (3.3.1), the system is considered as a free vibration system under damping, so equation (3.3.1) can be replaced by

$$m\ddot{x}(t) + c\dot{x}(t) + kx(t) = 0 \tag{3.3.2}$$

The solution of equation (3.3.2) may be written with a standard form as

$$x(t) = Ae^{bt} \tag{3.3.3}$$

where A is a constant defined by the initial condition.

Substituting equation (3.3.3) into equation (3.3.2), the equation of motion can be written as

$$\left(mb^2 + cb + k\right)Ae^{bt} = 0 \tag{3.3.4}$$

When the system is undamped, c is equal to zero, and equation (3.3.3) becomes

$$x(t) = Ae^{i\omega_n t} \tag{3.3.5}$$

where ω_n is the undamped natural frequency, because the system undergoes oscillatory motion at this frequency without decay.

Thus equation (3.3.4) becomes

$$\left(-m\omega_n^2 + k\right)Ae^{i\omega_n t} = 0 \tag{3.3.6}$$

Solving equation (3.3.6) gives

$$k = m\omega_n^2 \tag{3.3.7}$$

Therefore, the undamped natural frequency is obtained as

$$\omega_n = \sqrt{\frac{k}{m}} \tag{3.3.8}$$

and the eigenvalue λ is defined as

$$\lambda = \omega_n{}^2 = \frac{k}{m} \tag{3.3.9}$$

Rearranging equation (3.3.4) with equation (3.3.9),

$$b^2 + \frac{c}{m}b + \omega_n{}^2 = 0 \tag{3.3.10}$$

Therefore

$$b = -\frac{c}{2m} \pm \sqrt{\left(\frac{c}{2m}\right)^2 - \omega_n{}^2} \tag{3.3.11}$$

If the value of the damping coefficient c is equal to zero, the motion of the system is undamped and equation (3.3.11) is

$$b = \pm i\omega_n \tag{3.3.12}$$

Using equation (3.3.12), equation (3.3.3) may be written as

$$x(t) = A_1 e^{i\omega_n t} + A_2 e^{-i\omega_n t} \tag{3.3.13}$$

since

$$e^{\pm i\omega_n t} = \cos\omega_n t \pm i \sin\omega_n t \tag{3.3.14}$$

then

$$x(t) = B_1 \sin\omega_n t + B_2 \cos\omega_n t \tag{3.3.15}$$

or

$$x(t) = B\sin(\omega_n t + \alpha) \tag{3.3.16}$$

where $B = \sqrt{B_1{}^2 + B_2{}^2}$ and α is the phase angle.

The constants B, B_1, and B_2 of equation (3.3.15) and (3.3.16) may be obtained from the initial conditions such as the values of the displacement and velocity

at zero time. For example, if the initial values of displacement x(0) and velocity $\dot{x}(0)$ are substituted into equations (3.3.15), then

$$B = \sqrt{B_1^{\,2} + B_2^{\,2}} = \sqrt{\left(\frac{\dot{x}(0)}{\omega_n}\right)^2 + x(0)^2} \tag{3.3.17}$$

The unit of the natural frequency ω_n is radians per second (rad/sec), so the frequency in Hz is given by

$$f = \frac{\omega_n}{2\pi} \tag{3.3.18}$$

And the natural period of vibration is

$$T = \frac{1}{f} = \frac{2\pi}{\omega} \tag{3.3.19}$$

Considering the damped motion when the viscous damping coefficient c of equation (3.3.11) is non-zero.

If, $c < 2m\omega_n$

$$\left(\frac{c}{2m}\right)^2 - \omega_n^{\,2} < 0 \tag{3.3.20}$$

It can be seen from equation (3.3.11) that b will contain imaginary terms giving rise to oscillatory motion. This is the underdamped condition. For this case the solution of equation (3.3.2) is

$$x(t) = e^{-\frac{c}{2m}}\left(C_1 \sin\omega_d t + C_2 \cos\omega_d t\right) \tag{3.3.21}$$

where ω_d is the damped natural frequency.

If, $c = 2m\omega_n$

$$\left(\frac{c}{2m}\right)^2 - \omega_n{}^2 = 0 \tag{3.3.22}$$

which describes the critical damping condition. In this case the critical viscous damping coefficient c_c is obtained as

$$c_c = 2m\omega_n \tag{3.3.23}$$

and the viscous damping ratio ζ is defined as

$$\zeta = \frac{c}{c_c} = \frac{c}{2m\omega_n} \tag{3.3.24}$$

When ζ has the very small value of $\zeta < 0.1$, the system is almost the same as an undamped system. Increasing the value of ζ to 1, the system becomes critically damped and returns quickly to static equilibrium.

Using equation (3.3.24), equation (3.3.21) becomes

$$x(t) = e^{-\zeta\omega_n t}\left(C_1 \sin\omega_d t + C_2 \cos\omega_d t\right) \tag{3.3.25}$$

or

$$x(t) = Ce^{-\zeta\omega_n t}\sin\left(\omega_d t + \alpha\right) \tag{3.3.26}$$

where, C_1, C_2 and C are the arbitrary constants depending on the initial displacement and velocity.

Substituting equation (3.3.24) into equation (3.3.11), b may be written as

$$b = -\zeta\omega_n \pm \sqrt{\left(\zeta\omega_n\right)^2 - \omega_n{}^2} \tag{3.3.27}$$

or

$$b = -\zeta\omega_n \pm i\omega_d \tag{3.3.28}$$

where

$$\omega_d = \omega_n \sqrt{1-\zeta^2} \tag{3.3.29}$$

Figure 3-3 shows that the amplitudes x_1, x_2, $\cdots$ x_n, etc., occur in successive time intervals T.

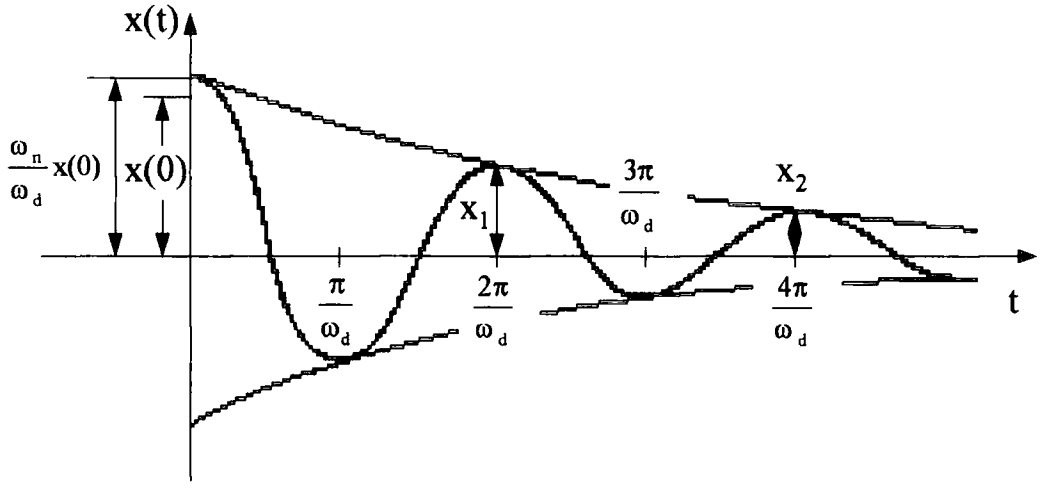

Figure 3-3. Free vibration response of damped system

The ratio of successive peaks is obtained by combining equations (3.3.21) and (3.3.24),

$$\frac{x_n}{x_{n+1}} = \frac{e^{-ct/2m}}{e^{-c(t+T)/2m}} = e^{2\pi\zeta(\omega_n/\omega_d)} \tag{3.3.30}$$

The natural logarithm of this ratio is called the logarithmic decrement δ,

$$\delta = \ln\left(\frac{x_n}{x_{n+1}}\right) = 2\pi\zeta\left(\frac{\omega_n}{\omega_d}\right) \tag{3.3.31}$$

Substituting equation (3.3.29) in equation (3.3.31) gives

$$\delta = \frac{2\pi\zeta}{\sqrt{1-\zeta^2}} \tag{3.3.32}$$

when ζ has a small value, $\delta \approx 2\pi\zeta$, therefore

$$\zeta = \frac{\delta}{2\pi} \tag{3.3.33}$$

If, $c > 2m\omega_n$

$$\left(\frac{c}{2m}\right)^2 - \omega_n{}^2 > 0 \tag{3.3.34}$$

which means the overdamped system. For this case equation (3.3.11) may be written as

$$b = -\zeta\omega_n \pm \omega_{od} \tag{3.3.35}$$

in which

$$\omega_{od} = \omega_n\sqrt{\zeta^2 - 1} \tag{3.3.36}$$

where $\zeta > 1$, and ω_{od} does not represent a frequency since the overdamped system is not oscillatory.

Therefore, the solution of the equation of motion becomes

$$x(t) = e^{-\zeta\omega_n t}\left(E_1 \sinh\omega_{od}t + E_2 \cosh\omega_{od}t\right) \tag{3.3.37}$$

where the constants E_1 and E_2 are evaluated from the initial conditions and the motion is not oscillatory. ω_{od}

3.3.1.2. Forced vibration system

In equation (3.3.1), if external force F(t) is equal to $F_o\sin(\omega t \pm \alpha)$ which has amplitude F_o and is applied as a steady state dynamic Sin function with a phase defined by angle α, the equation of motion may be written as

$$m\ddot{x}(t) + c\dot{x}(t) + kx(t) = F_o \sin(\omega t \pm \alpha) \qquad (3.3.38)$$

where ω is the forced frequency.

Note that in order to gain the values of natural frequencies, F_o may be set to zero to represent a system under free vibration.

The solution of equation (3.3.38) has two parts,

$$x(t) = x_c(t) + x_F(t) \qquad (3.3.39)$$

Where $x_c(t)$ is the complementary solution which is obtained from the solution of the equation of motion when the force is zero. This corresponds to the free vibration solution. $x_F(t)$ is the particular integral which is the direct solution from equation (3.3.38). This states the specific behaviour of the system which is caused by the dynamic force.

From equation (3.3.25), the complementary solution is

$$x_c(t) = e^{-\zeta\omega_n t}\left(C_1 \sin\omega_d t + C_2 \cos\omega_d t\right) \qquad (3.3.40)$$

To obtain $x_F(t)$, assuming that

$$x_F(t) = C_3 \cos\omega t + C_4 \sin\omega t \qquad (3.3.41)$$

Substituting equation (3.3.41) into equation (3.3.38), and equating the coefficients of $\cos\omega t$ and $\sin\omega t$ separately,

$$-m\omega^2 C_3 + c\omega C_4 + k C_3 = F_o \qquad (3.3.42)$$

$$-m\omega^2 C_4 - c\omega C_3 + k C_4 = 0 \qquad (3.3.43)$$

Constants C_3 and C_4 can be obtained from equations (3.3.42) and (3.3.43), then substituting C_3 and C_4 into equation (3.3.41) gives

$$x_F(t) = \frac{F_o \cos(\omega t - \alpha)}{\sqrt{\left(k - m\omega^2\right)^2 + c^2\omega^2}} \tag{3.3.44}$$

and

$$\tan\alpha = \frac{c\omega}{k - m\omega^2} \tag{3.3.45}$$

Substituting equation (3.3.24) into equations (3.3.44) and (3.3.45) gives

$$x_F(t) = \frac{F_o}{k} \frac{\cos(\omega t - \alpha)}{\sqrt{\left(1 - r^2\right)^2 + (2\zeta r)^2}} \tag{3.3.46}$$

$$\alpha = \tan^{-1}\left(\frac{2\zeta r}{1 - r^2}\right) \tag{3.3.47}$$

where r is the frequency ratio defined as

$$r = \frac{\omega}{\omega_n} \tag{3.3.48}$$

therefore

$$x(t) = x_c(t) + x_F(t)$$

$$= e^{-\zeta\omega_n t}\left(C_1 \sin\omega_d t + C_2 \cos\omega_d t\right) + \frac{F_o}{k} \frac{\cos(\omega t - \alpha)}{\sqrt{\left(1 - r^2\right)^2 + (2\zeta r)^2}} \tag{3.3.49}$$

In a system with damping, $x_c(t)$ reduces quickly to zero and is usually neglected. Therefore,

$$x(t) = \frac{F_o}{k} \frac{\cos(\omega t - \alpha)}{\sqrt{\left(1 - r^2\right)^2 + (2\zeta r)^2}} \tag{3.3.50}$$

In equation (3.3.50) it should be noted that F_o/k equals the displacement x_s of the system subjected to a static force F_o. Thus

$$\frac{x(t)}{x_s} = \frac{\cos(\omega t - \alpha)}{\sqrt{(1-r^2)^2 + (2\zeta r)^2}} \tag{3.3.51}$$

The maximum value is when $\cos(\omega t - \alpha) = 1$, so equation (3.3.51) becomes

$$\left(\frac{x(t)}{x_s}\right)_{max} = \frac{1}{\sqrt{(1-r^2)^2 + (2\zeta r)^2}} \tag{3.3.52}$$

This is called the dynamic magnification factor.

The importance of vibration in structures arises mainly from the large values of $x(t)/x_s$ experienced in practice when ω/ω_n has a value near unity. This means that even a small harmonic force can produce a large amplitude of vibration.[25] This is the phenomenon which is known as resonance. And the resonant frequency for damped systems is $\omega_n\sqrt{1-2\zeta^2}$. This is the frequency at which the magnification is greatest. The maximum value of $x(t)/x_s$ actually occurs at values of ω/ω_n less than unity. For small values of ζ, equation (3.3.52) can be written as

$$\left(\frac{x(t)}{x_s}\right)_{max} = \frac{1}{2\zeta} \tag{3.3.53}$$

Resonance is a phenomenon related to forced vibration, generated by some input force, whereas natural frequencies are phenomena of free vibration. Resonance is very important in practice because it involves large amplitude

response to excitation, and can cause serious problems such as a structural failure.[26]

3.3.2. MDOF Vibration System

Figure 3-4 shows a forced and damped multi degrees of freedom(MDOF) system.

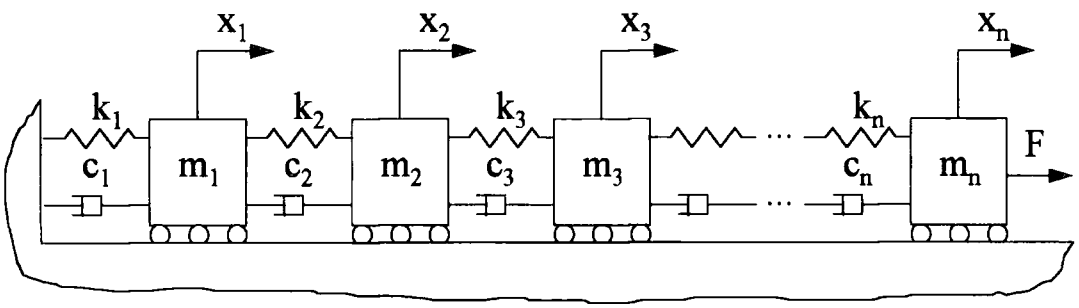

Figure 3-4. MDOF forced and damped vibration system

Equations of motion for the n masses may be written as follows,

$$\text{First mass}: m_1\ddot{x}_1 + c_1\dot{x}_1 + k_1x_1 - k_2(x_2 - x_1) - c_2(\dot{x}_2 - \dot{x}_1) = F_1 \quad (3.3.54)$$

$$j^{th}\ \text{mass}: m_j\ddot{x}_j + c_j\dot{x}_j + k_j(x_j - x_{j-1}) - k_{j+1}(x_{j+1} - x_j) - c_{j+1}(\dot{x}_{j+1} - \dot{x}_j) = F_j \quad (3.3.55)$$

$$\text{Last mass}: m_n\ddot{x}_n + c_n\dot{x}_n + k_n(x_n - x_{n-1}) = F_n \quad (3.3.56)$$

where, F_1 is the force which is loaded on mass m_1,

F_j is the force which is loaded on mass m_j,

and F_n is the force which is loaded on mass m_n.

These equations may be written in matrix form[27]

$$[\mathbf{M}]\{\ddot{\mathbf{x}}\}+[\mathbf{C}]\{\dot{\mathbf{x}}\}+[\mathbf{K}]\{\mathbf{x}\}=\{\mathbf{F}\} \tag{3.3.57}$$

where, if n=3, for example,

the mass matrix is

$$[\mathbf{M}]=\begin{bmatrix} m_1 & 0 & 0 \\ 0 & m_2 & 0 \\ 0 & 0 & m_3 \end{bmatrix}$$

the damping coefficient matrix is

$$[\mathbf{C}]=\begin{bmatrix} (c_1+c_2) & -c_2 & 0 \\ -c_2 & (c_2+c_3) & -c_3 \\ 0 & -c_3 & c_3 \end{bmatrix}$$

the stiffness matrix is

$$[\mathbf{K}]=\begin{bmatrix} (k_1+k_2) & -k_2 & 0 \\ -k_2 & (k_2+k_3) & -k_3 \\ 0 & -k_3 & k_3 \end{bmatrix}$$

A n degrees of freedom system has n eigenvalues, which means the system has n natural frequencies. If the viscous damping ratio ζ has small value, it may be assumed that maximum forced response will occur when ω is one of the natural frequencies.

If the system is in undamped free vibration, equation (3.3.57) can be written as

$$[\mathbf{M}]\{\ddot{\mathbf{x}}\}+[\mathbf{K}]\{\mathbf{x}\}=\mathbf{0} \tag{3.3.58}$$

where

$$\{\ddot{\mathbf{x}}\}=-\omega^2\{\mathbf{x}\} \tag{3.3.59}$$

can be stated for a simple harmonic motion.

Substituting equation (3.3.59) into equation (3.3.58) gives

$$-\omega^2[\mathbf{M}]\{\mathbf{x}\} + [\mathbf{K}]\{\mathbf{x}\} = \mathbf{0}$$

or

$$[\mathbf{K} - \omega^2\mathbf{M}]\{\mathbf{x}\} = \mathbf{0} \tag{3.3.60}$$

Equation (3.3.60) represents a frequency eigenvalue problem, and the vector $\{\mathbf{x}\}$ which corresponds to a particular mode of vibration is called an eigenvector.

As in the frequency eigenvalue analysis of a MDOF system, the solution to equation (3.3.60) can be found. This can be solved by recognising that, because of the zero right hand side, the only non-trivial solution to the system is one in which

$$|\mathbf{K} - \omega^2\mathbf{M}| = \mathbf{0} \tag{3.3.61}$$

Equation (3.3.61) is called the frequency equation which can be solved to find the natural frequencies.

The shape of each mode for each natural frequency can be defined by the eigenvector $\{\mathbf{x}\}$. Considering an n degrees of freedom system, if $\{\phi_i\}$ is the ith displacement eigenvector, then the mode shape is given by

$$\{\phi_i\} = \begin{Bmatrix} \phi_{1i} \\ \phi_{2i} \\ \vdots \\ \phi_{ni} \end{Bmatrix} \tag{3.3.62}$$

Therefore, a square mode shape matrix $[\phi]$ may be written to include the n mode shapes by equation (3.3.63).

$$[\phi] = \begin{Bmatrix} \phi_{11} & \cdots & \phi_{1i} & \cdots & \phi_{1n} \\ \phi_{21} & \cdots & \phi_{2i} & \cdots & \phi_{2n} \\ \vdots & & \vdots & & \vdots \\ \phi_{n1} & \cdots & \phi_{ni} & \cdots & \phi_{nn} \end{Bmatrix} \tag{3.3.63}$$

In a forced vibration system, the forced frequency influences to the forced response. If the forced frequency is very close to one of the system natural frequencies, the resonance which is mentioned in section 3.3.1.2 is occurred. The modal superposition method is that the displaced shape of a structure can be constructed by the sum of the free vibration mode shapes. For an n DOF system, there will be n independent displacement patterns which are considered to be generalised coordinates Y_1, Y_2, ..., Y_n. Thus, by using the mode shape matrix $[\phi]$, the local coordinates $\{\mathbf{x}\}$ which is considered previously may be written as

$$\{\mathbf{x}\} = [\phi]\{\mathbf{Y}\} \tag{3.3.64}$$

Therefore, equation (3.3.57) may be given as

$$[\mathbf{M}][\phi]\{\ddot{\mathbf{Y}}\} + [\mathbf{C}][\phi]\{\dot{\mathbf{Y}}\} + [\mathbf{K}][\phi]\{\mathbf{Y}\} = \{\mathbf{F}\} \tag{3.3.65}$$

By premultiplying by $[\phi]^T$, the orthogonality properties of the mode shapes allow much simplification of the system. In order to achieve the fullest simplification, it is necessary to consider the damping matrix [**C**]. While it can be shown that the mode shape vectors are orthogonal with respect to the mass and stiffness matrices, [**M**] and [**K**], no such proof is available in general for [**C**]. However, this can be overcome by making the assumption that [**C**] may

be constructed as the sum of [**M**] and [**K**], multiplied by scalar coefficients. This is termed proportional damping, or Rayleigh damping, and extends the orthogonality properties to the damping matrix. It can be seen that by considering the orthogonality relations, equation (3.3.65) reduces to a set of equations of the form

$$M_i^*\ddot{\xi}_i + C_i^*\ddot{\xi}_i + K_i^*\xi_i = 0 \qquad (3.3.66)$$

where $M_i^* = \phi_i^T M \phi_i$ is the generalised modal mass for mode *i*, and the generalised modal stiffness and damping terms are similarly constructed by replacing [**M**] with [**C**] and [**K**] respectively. ξ_i is termed a modal participation factor, and this determines the contribution of mode *i* to the overall response. The importance of equation (3.3.66) is that all such equations for the different modes are uncoupled and may be solved independently.

4. Finite Element Method (FEM)

4.1. General Concept of The Finite Element Method

The finite element method(FEM) is a numerical solution procedure for the differential equations of physics or engineering. The FEM can be applied to various fields, for instance, the analysis of the frame structure of an aircraft or an automobile, a complicated thermal system, such as a nuclear power plant, or the analysis of all sort of fluid dynamics. Other application areas include not only compressible gas flow but also electrostatics, lubrication problems, and the analysis of vibrating systems.[4]

The modern concept of the finite element method came from the approximate analysis of the structural elasticity problem which is discussed by Timoshenko[28] . The term 'finite element' was wired by Clough[29]. In the early 1950s work using the FEM was first published by Turner, Clough, Martin, and Topp[30]. At the same time Argyris and Kelsey[31] presented the FEM in their publications. These publications led the significant development of the FEM among the researchers who worked principally in structural mechanics. In 1963, Melosh[32] contributed theoretically to the FEM by showing that the FEM was a variation of the Rayleigh-Ritz method. The FEM was applied to the Laplace and the Poisson equations, and thus Zienkiewicz and Cheung[33], Visser[34], Wilson and Nickell[35] applied the FEM to conductive heat transfer

and some limited problems in fluid mechanics in their publications. In 1969, Szabo and Lee[36] enlarged the range of applications for the FEM to the structural mechanics, heat transfer, fluid dynamics by using Galerkin's method or the least-squares approach. Nowadays with the development of both the numerical procedures and computer systems, the FEM has been applied to most engineering and industrial fields.

The major concept of the finite element method is that any continuous quantity, such as temperature, pressure, or displacement, may be approximated as a discrete model composed of a group of piecewise continuous functions which are defined over a finite number of subdomains.

The discrete model is composed as follows[4] :

- Finite points in the domain are identified. These points are defined as nodal points or nodes.
- The value of the continuous quantity at each nodal point is denoted as a variable which is to be determined.
- The domain is divided into finite subdomains named finite elements. These elements are connected at common nodal points and approximated according to the shape of the domain.
- The continuous quantity is identified over each element by a polynomial that is defined in terms of the nodal values of the continuous quantity. A different polynomial is defined for each element, but the element

polynomials are selected by virtue of the requirement that continuity is maintained across element boundaries.

Several advantageous properties of the finite element method include[4] :

- The material properties in adjacent elements do not have to be the same. This means that the method can be applied to bodies composed of several materials.
- Irregularly shaped boundaries can be simplified using straight sided elements or matched exactly using elements with curved boundaries. Therefore, the method is not limited to simple shapes which have easily defined boundaries.
- The size of the elements can be varied. This property allows the element grid to be expanded or refined in accordance with the need.
- There are no difficulties in applying boundary conditions such as a distributed load or zero displacement in this method. Mixed boundary conditions can be easily applied and handled.
- The above properties can be incorporated into one general computer program for a particular subject. For example, a general computer program for steady state dynamics is capable of solving problems of this type. Only the availability of computer memory and the computational costs are the limiting factors to solve a problem.

4.2. Finite Element Types and Shape Functions

Instead of the real displacement, the approximate displacement ϕ at any point within an element may be expressed by an appropriate shape function, given the displacements at the element nodes. Because this is much easier than considering the real case to describe the deformation. For example, the three-noded triangular element may be expressed as

$$\phi = N_1\phi_1 + N_2\phi_2 + N_3\phi_3 \tag{4.2.1}$$

where ϕ_1, ϕ_2, ϕ_3 are the displacements at the three nodes, and N_1, N_2, N_3 are the shape functions for nodes 1, 2 and 3 respectively. Developing equation (4.2.1) to the general case, an n-noded element may be written as

$$\phi = \sum_{i=1}^{n} N_i\phi_i \tag{4.2.2}$$

The shape function is unity at the node to which it refers only, and zero at all other nodes.

In general, equation (4.2.2) may be written in matrix form

$$\{\phi\} = [\mathbb{N}]\{\phi_e\} \tag{4.2.3}$$

where $\{\phi\}$ is a vector containing the displacement components at any point in the element, $[\mathbb{N}]$ is a shape function matrix, and $\{\phi_e\}$ is a vector containing the nodal displacements. The size of these matrices is dependent on both the number of nodes in the element and the number of degrees of freedom for which the displacements are active.

In general, the shape function is a polynomial, and its order is determined by the element type.

In 1972, Oden[37] classified finite elements into three groups defined as simplex, complex, and multiplex according to the order of the element polynomial. The simplex elements have an approximating polynomial that consists of the constant term plus the linear terms. The number of coefficients in the polynomial is equal to the dimension of the coordinate space plus one. For an one-dimensional simplex element such as a line segment, the polynomial function may be written as

$$\phi = \alpha_1 + \alpha_2 x \tag{4.2.4}$$

Figure 4-1 shows three types of the one-dimensional line element.

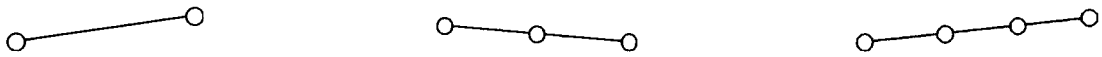

(a) linear **(b) quadratic** **(c) cubic**

Figure 4-1. One-dimensional line elements

This element is normally used in one-dimensional heat transfer problems and structural problems of welding or mounting conditions.

The two-dimensional element has two general types. A triangular element may have a different number of nodes according to the order of the element. In fact a 3-noded triangular element is a very poor element. It is more common to see the 6-noded triangular element used. Likewise, the 8-noded

quadrilateral element is at least as common as the 4-noded linear quadrilateral element, though the 4-noded quadrilateral element is not as poor as the 3-noded triangular element.

The polynomial

$$\phi = \alpha_1 + \alpha_2 x + \alpha_3 y \tag{4.2.5}$$

is the simplex function for the two-dimensional triangular element. The polynomial is linear in x and y and contains three coefficients because the triangle has three nodes.

Three types of the two-dimensional triangular element are presented in figure 4-2.

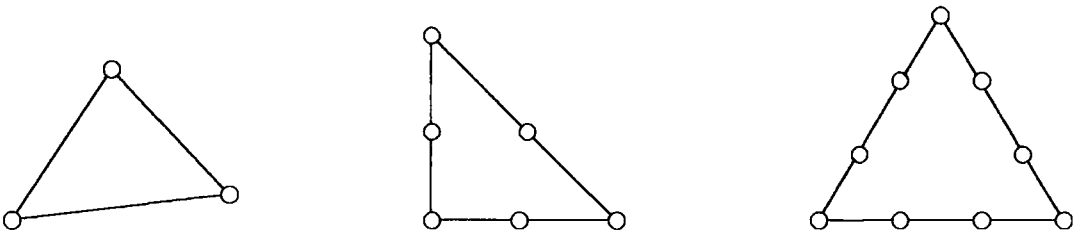

(a) linear **(b) quadratic** **(c) cubic**

Figure 4-2. Two-dimensional triangular elements

And the interpolation polynomial for the tetrahedron is

$$\phi = \alpha_1 + \alpha_2 x + \alpha_3 y + \alpha_4 z \tag{4.2.6}$$

The complex elements use a polynomial function consisting of the constant and linear terms plus second, third, and higher-order terms as they are needed. The complex elements can have the same shapes as the simplex

elements, but they have additional boundary nodes and may also have internal nodes. The primary difference between the simplex and complex elements is that the number of nodes in a complex element is greater than one plus the dimension of the coordinate space. An interpolating polynomial for a two-dimensional complex triangular element (quadratic triangular element) is

$$\phi = \alpha_1 + \alpha_2 x + \alpha_3 y + \alpha_4 x^2 + \alpha_5 xy + \alpha_6 y^2 \qquad (4.2.7)$$

This equation has six coefficients, therefore, the element must have six nodes. It is also complete through the second order terms.

Considering a cubic triangular element, the interpolating polynomial is

$$\phi = \alpha_1 + \alpha_2 x + \alpha_3 y + \alpha_4 x^2 + \alpha_5 xy + \alpha_6 y^2 + \alpha_7 x^3 + \alpha_8 x^2 y + \alpha_9 xy^2 + \alpha_{10} y^3 \qquad (4.2.8)$$

The multiplex elements also use polynomials containing higher order terms, but the element boundaries must be parallel to the coordinate axes to achieve inter-element continuity. The element boundaries of the simplex and complex elements are not subjected to this restriction.

The quadrilateral element is a multiplex element. And the rectangular element is a special case of the quadrilateral.

Considering about the linear quadrilateral element, then the interpolation polynomial for the four-node rectangular element is

$$\phi = \alpha_1 + \alpha_2 x + \alpha_3 y + \alpha_4 xy \qquad (4.2.9)$$

The curvilinear coordinate system, $\xi\eta$, which is shown in figure 4-3, is used instead of the natural coordinate system to describe the polynomial of the quadrilateral element.[4] In figure 4-3, the line segment $\xi = 1/2$ is not parallel

to the η axis, but it connects points c and d which are the midpoints of the upper and lower chords bounded by $\xi = 0$ and $\xi = 1$.

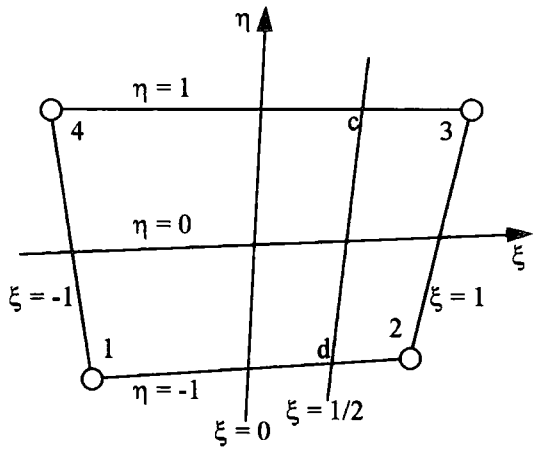

Figure 4-3. $\xi\eta$ curvilinear coordinate system

This quadrilateral element is referred to as the linear quadrilateral because the interpolating polynomial is linear in ξ along lines of constant η and vice versa. Quadrilateral elements with 8 and 12 nodes are referred to as the quadratic and cubic elements because the interpolating polynomials are either quadratic or cubic, along lines of constant ξ or constant η. The interpolating polynomials for these two elements are

$$\phi = \alpha_1 + \alpha_2\xi + \alpha_3\eta + \alpha_4\xi\eta + \alpha_5\xi^2 + \alpha_6\eta^2 + \alpha_7\xi^2\eta + \alpha_8\xi\eta^2 \qquad (4.2.10)$$

$$\phi = \alpha_1 + \alpha_2\xi + \alpha_3\eta + \alpha_4\xi\eta + \alpha_5\xi^2 + \alpha_6\eta^2 + \alpha_7\xi^2\eta + \alpha_8\xi\eta^2 + \alpha_9\xi^3 + \alpha_{10}\eta^3 + \alpha_{11}\xi^3\eta + \alpha_{12}\xi\eta^3 \qquad (4.2.11)$$

Figure 4-4 shows three types of the two-dimensional quadrilateral element.

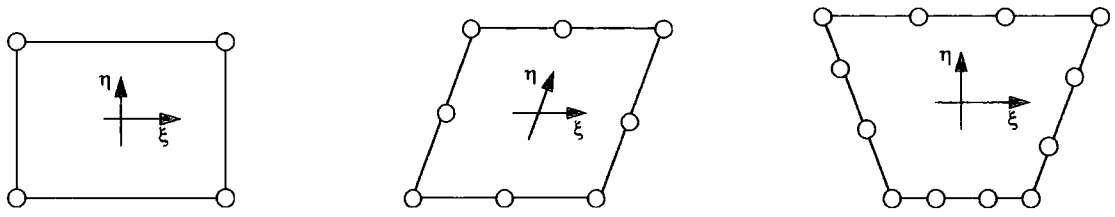

(a) linear (b) quadratic (c) cubic

Figure 4-4. Two-dimensional quadrilateral elements

The tetrahedron element and the parallelepiped(hexahedral) element are the common three-dimensional elements.

The most stable element for the thin shell panel structure is the quadrilateral element. New element formulations are continually under development, for example, a new four-node quadrilateral element which can effectively describe the bending behaviour of thin plates is described by Roufaeil in 1993.[38] The common quadrilateral element uses quadrilateral shape functions. Figure 4-5 shows other particular types of a quadrilateral element which is constructed by triangular elements.

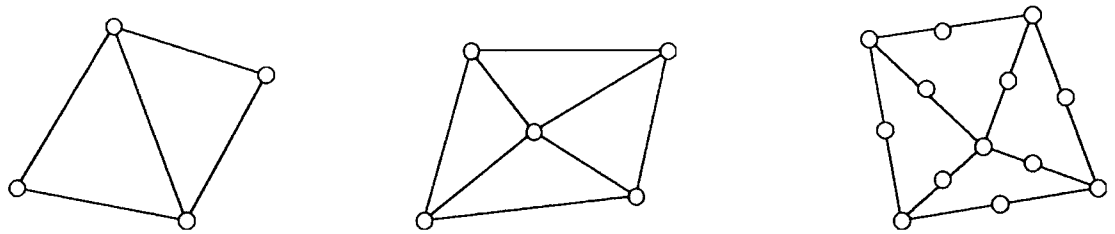

Figure 4-5. Several types of the quadrilateral element constructed by triangular elements

4.3. Stiffness Matrix

The mass and stiffness matrices for each element reflect the fact that degrees of freedom are shared between elements. For instance, if two bar elements join at node 2, the displacement at node 2 becomes part of two sets of equations. These sets of equations need to be solved together to find the displacement value which will satisfy the equations for both elements. Considering the whole model, all of the stiffness and mass matrices need to be combined into one large set of simultaneous equations, which may be written in matrix form such as follows,

$$[\mathbf{M}]\{\ddot{\mathbf{x}}\} + [\mathbf{C}]\{\dot{\mathbf{x}}\} + [\mathbf{K}]\{\mathbf{x}\} = \{\mathbf{F}\} \tag{4.3.1}$$

where [**M**], [**C**] and [**K**] are square matrices of size (n x n) for a n degree of freedom problem. Vectors {**x**} and {**F**} contain the displacements and forces considered at each degree of freedom. In this respect the FEM looks similar to the MDOF vibration analysis procedures. But the difference comes in the generality; the mass and stiffness matrices may be computed for a large number of standard shape elements in FEM. A FEM software package such as NASTRAN or ABAQUS is supplied with libraries of many types of elements : bars, beams, triangular plane stress, quadrilateral plane stress, triangular and quadrilateral thin shells, thick shells, tetrahedral solids, wedge shaped solids, and hexahedral (cuboid) solids. These can be used with different orders (constant, linear, quadratic strain, etc.), and as such researchers have access to a wide choice of elements.

If the system is in undamped free vibration, equation (4.3.1) can be written as

$$[\mathbb{M}]\{\ddot{\mathbb{x}}\} + [\mathbb{K}]\{\mathbb{x}\} = \mathbf{0} \tag{4.3.2}$$

where

$$\{\ddot{\mathbb{x}}\} = -\omega^2\{\mathbb{x}\} \tag{4.3.3}$$

can be stated for a simple harmonic motion from equation (3.3.8).

Substituting equation (4.3.3) into equation (4.3.2) gives

$$-\omega^2[\mathbf{M}]\{\mathbf{x}\} + [\mathbf{K}]\{\mathbf{x}\} = \mathbf{0}$$

or

$$[\mathbf{K} - \omega^2\mathbf{M}]\{\mathbf{x}\} = \mathbf{0} \tag{4.3.4}$$

As in the frequency eigenvalue analysis of a MDOF system, the solution to equation (4.3.4) can be found. This can be solved by recognising that, because of the zero right hand side, the only non-trivial solution to the system is one in which

$$|\mathbf{K} - \omega^2\mathbf{M}| = \mathbf{0} \tag{4.3.5}$$

The element stiffness matrix may be derived easily by the method of virtual work.[4]

By using an expression for the displacements at any point in the element, an expression for the strain at any point in the element can be developed. Using equation (4.2.3), the matrix form of the strain-displacement relationships for the two-dimensional case may be written as

$$\{\varepsilon\} = \begin{Bmatrix} \varepsilon_x \\ \varepsilon_y \\ \gamma_{xy} \end{Bmatrix} = [\mathbf{S}]\{\phi\} = [\mathbf{S}][\mathbf{N}]\{\phi_e\} \tag{4.3.6}$$

where [**S**] is a matrix containing the differential operators required to obtain the strains from the displacements. By defining a matrix [**B**] which is derived by performing the proper differentiation of [**N**], equation (4.3.6) can be written as

$$\{\varepsilon\} = [\mathbf{S}][\mathbf{N}]\{\phi_e\} = [\mathbf{B}]\{\phi_e\} \tag{4.3.7}$$

From equation (3.1.1), the stress-strain relationships may be used to find the stresses at any point in the element. In a two-dimensional linear elastic case, the matrix form of the stress gives

$$\{\sigma\} = \begin{Bmatrix} \sigma_x \\ \sigma_y \\ \tau_{xy} \end{Bmatrix} = [\mathbf{D}]\{\varepsilon\} = [\mathbf{D}][\mathbf{B}]\{\phi_e\} \tag{4.3.8}$$

where [**D**] is the elasticity matrix which relates the stress components to the strain components.

By the principle of virtual work for nodal displacement vector $\{\phi_e\}$, the internal work W_I is equal to the external work W_E. Where, the internal work W_I may be obtained by integrating the virtual stresses $\{\sigma\}$ and the virtual strains $\{\varepsilon\}$ over the total volume of the element V.

$$W_I = \int_V \{\varepsilon\}^T \{\sigma\} dV \tag{4.3.9}$$

Substituting equations (4.3.7) and (4.3.8) into equation (4.3.9) gives

$$W_I = \int_V \left([B]\{\phi_e\}\right)^T [D][B]\{\phi_e\} dV \tag{4.3.10}$$

Since $\{\phi_e\}$ contains the nodal displacements which are constant through the element, equation (4.3.10) can be rewritten as

$$W_I = \{\phi_e\}^T \int_V [B]^T [D][B] dV \{\phi_e\} \tag{4.3.11}$$

The external work W_E is defined as the product of the nodal displacements vector $\{\phi_e\}$ and the nodal forces vector $\{F\}$ which is applied to the element

$$W_E = \{\phi_e\}^T \{F\} \tag{4.3.12}$$

Combining equations (4.3.11) and (4.3.12) gives

$$\{F\} = \int_V [B]^T [D][B] dV \{\phi_e\} \tag{4.3.13}$$

Defining the element stiffness matrix $[K]$ as

$$[K] = \int_V [B]^T [D][B] dV \tag{4.3.14}$$

then equation (4.3.13) may be written as

$$\{F\} = [K]\{\phi_e\} \tag{4.3.15}$$

5. Experiment

In the case of an actual vehicle, the viscous damping ratio of the door panel has been obtained by a simple experiment as follows,

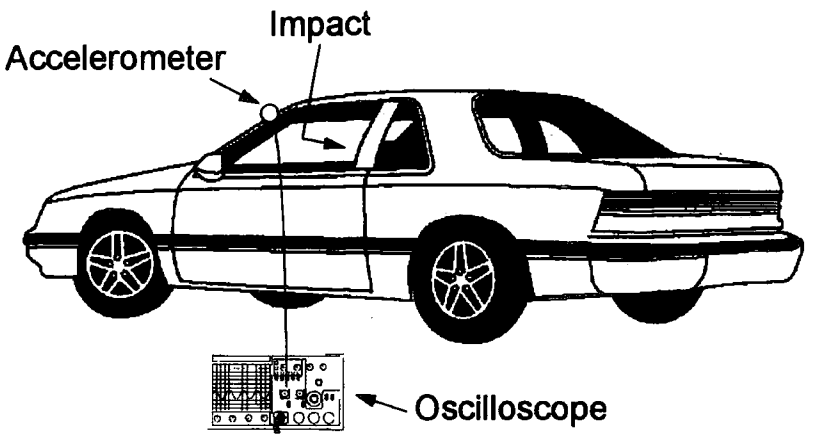

Figure 5-1. Experiment for measuring oscillation

The amplitude of each oscillation can be measured by oscilloscope, so the logarithmic decrement is obtained from equation (3.3.31).

The amplitude of the second oscillation was found to be 60 percent of the first oscillation amplitude, from equation (3.3.31) δ is

$$\delta = \ln\left(\frac{x_n}{x_{n+1}}\right) = \ln\left(\frac{100}{60}\right) = 0.51$$

But there were some significant problems in capturing and accurately visualising the transient acceleration response. The value of 60 percent was an

approximation based on noisy data and should be considered as perhaps 60 ± 10 %.

Substituting $\delta = 0.51$ into equation (3.3.33),

$$\zeta = \frac{\delta}{2\pi} = \frac{0.51}{2\pi} \approx 0.081$$

the viscous damping ratio 0.081 is obtained.

The value of ζ was established through the decay in oscillations of the fundamental mode, and It may not be applicable over the entire frequency range. However this study is comparative in nature and it would be expected to have reached the same conclusions on reinforcement design even if the value of ζ which is adopted was slightly in error.

This experiment was carried out on the Durham hybrid vehicle. Although the value of viscous damping ratio is variable according to vehicles, the viscous damping ratio 0.081 was applied to all analyses in this thesis.

6. Modelling and Analysis

6.1. Modelling

The original model and models of several reinforcement types have been produced using ABAQUS, commercial finite element code. Continuum elements, based on elasticity theory, are employed.

The deformation mode is assumed to be linear-elastic; in this case there are no plastic stresses and plastic strains. The case of inelastic deformation by repeated loading of air pressure is only occurred on fatigue crack. This is not considered in the scope of this research.

In the case of the vehicle's door panel, the model is defined using thin shell elements which can describe the stress and strain states adequately as described in section 3.1.[39]

Thin shell theory[17] is the most appropriate to model the door panel assembly, which is constructed with thin panels including some spot welding points. Each panel of the assembly is divided into small thin shell elements. Welding points are modelled by using MPC(multi-point constraint)'s and a finite element discretisation of the door glass is fixed to the outer panel using further MPC's. MPC's are constructed by tying separate nodes of different parts to have identical displacement values. Most finite elements are the preferred

quadrilateral shape, but some parts are modelled by triangular elements unavoidably. All elements are quadratic in order.

The original CAD data of the door panel assembly are produced by CATIA which is the primary CAD software used in Hyundai. In order to import the CATIA data into ABAQUS-Pre, the modelling tool of ABAQUS, the data were exported from CATIA as IGES data in advance. Then by importing the IGES data into ABAQUS-Pre, it is ready for modelling.

In ABAQUS-Pre, the 'mesh-seed' function is generally applied to guide the finite element meshing, but in some cases, according to the shape of particular part, the 'mesh' or 'element' function can be selected appropriately.

It is very important that the proper number and size of the elements should be decided in terms of the purpose and accuracy of the analysis. This crucial aspect of finite element modelling is documented at great length in many texts and will not be described further here.[39]

The material of the door window is glass, and for all structural panels, the material is steel. Until recently, steel has continued to be the most general and useful material for a vehicle's structural panels in view of the cost, structural strength and manufacturability.

Figure 6-1 shows the vehicle door panel assembly which is studied in this research.

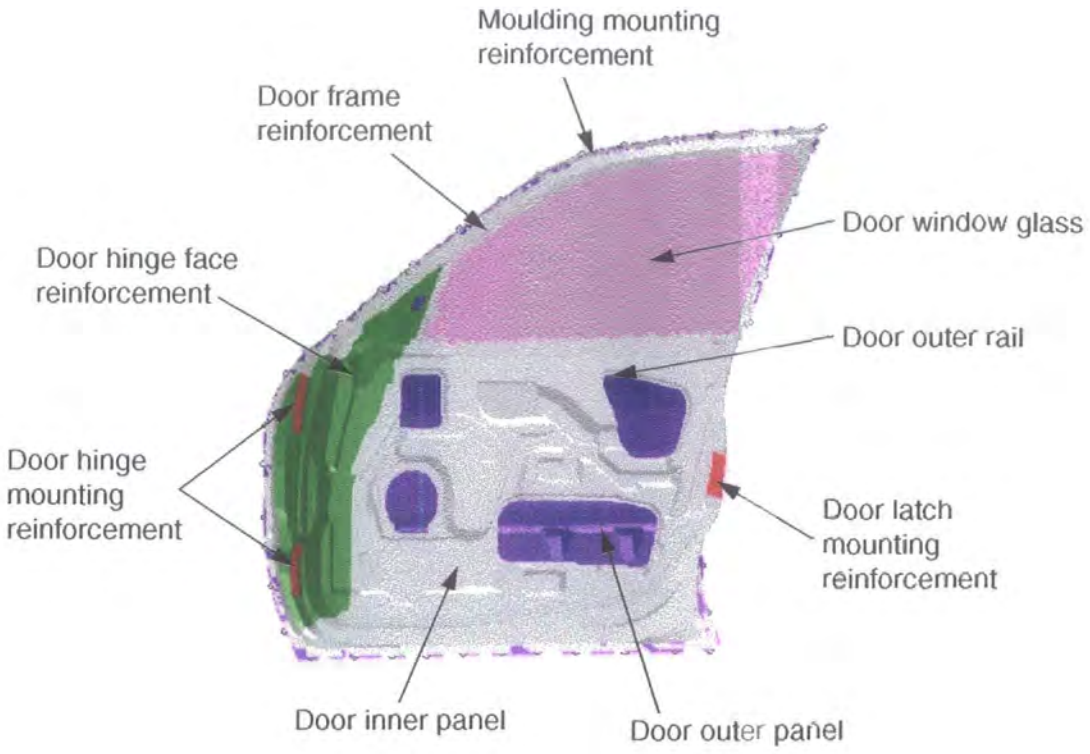

Figure 6-1. Parts of the door panel assembly

Each panel is given a thickness equal to the actual vehicle's door panel, with particular values as shown in table 6-1.

Part name	Panel thickness (mm)
Door outer panel	0.8
Door inner panel	0.8
Door frame reinforcement	1.2
Door outer rail	1.0
Door hinge face reinforcement	1.4
Door latch mounting reinforcement	1.0
Door hinge mounting reinforcement	2.0
Moulding mounting reinforcement	0.6
Door window glass	4.0

Table 6-1. Panel thickness of each part

The pipe reinforcements for side impact safety located in the below door belt region are not included in the model because they do not greatly influence this vibration analysis. The main concern is the vibrational deformation of the frame region only.

It should be noted that finite element tests have shown that the natural frequencies for the door panel with and without these assembled parts are similar, and therefore it may be deemed reasonable to omit these parts from the model for the purposes of this research. This will be further detailed later in section 7.2.

Figure 6-2 shows the finite element model of model 1 which is the original model before modifying the reinforcement. It contains 8448 thin shell elements and 8904 nodes. The numbers of nodes and elements of each parts and several reinforcements are presented in table 6-2.

For table 6-2, reinforcement 6 does not have finite elements, because it was created by addition 1.2mm to the thickness of the door inner panel.

For clarity, figure 6-3 shows the finite element models of the separate panels which make up the model.

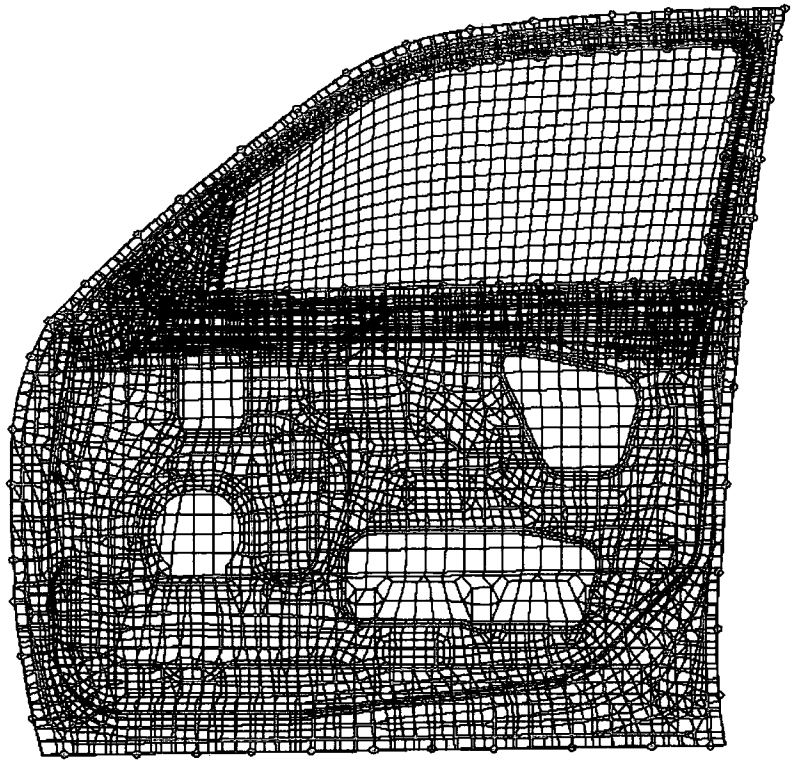

Figure 6-2. Finite element model of the original model (model 1)

Part name	Number of nodes	Number of elements
Moulding mounting reinforcement	192	96
Door frame reinforcement	1318	1047
Door window glass	688	612
Door hinge face reinforcement	809	749
Door hinge mounting reinforcement	80	62
Door inner panel	4122	3839
Door latch mounting reinforcement	30	20
Door outer panel	1849	1711
Door outer rail	377	312
MPC(multi-point constraints)	270	0
Total in the original model	8904	8448
Reinforcement 1	756	630
Reinforcement 2	321	243
Reinforcement 3	435	387
Reinforcement 4, reinforcement 9	887	757
Reinforcement 5	1712	1609
Reinforcement 7	903	737
Reinforcement 8	450	231

Table 6-2. The number of nodes and elements of each part

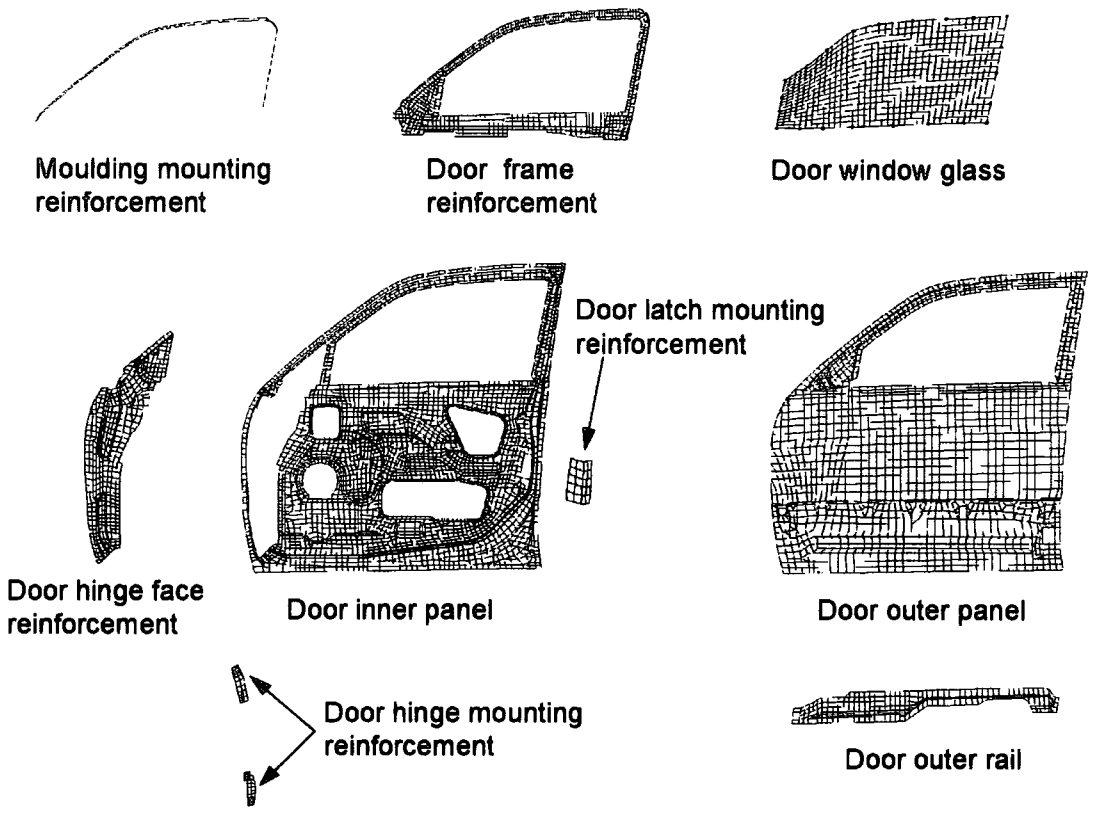

Figure 6-3. Finite element models of parts

Figures 6-4 to 6-13 present the shapes of reinforcements for each model.

Model 2 is the base model which is generated from the original model by removing the original frame reinforcement.

The thickness of the reinforcements is 1.2mm, but for reinforcement 8 (model 10), the thickness is 4.0mm.

After analysing the basic model, several further cases were investigated according to various changes of the panel assembly's geometry and the thickness of reinforcing material. This will be used as a basis for determining an optimum solution of high dynamic stiffness and low weight.

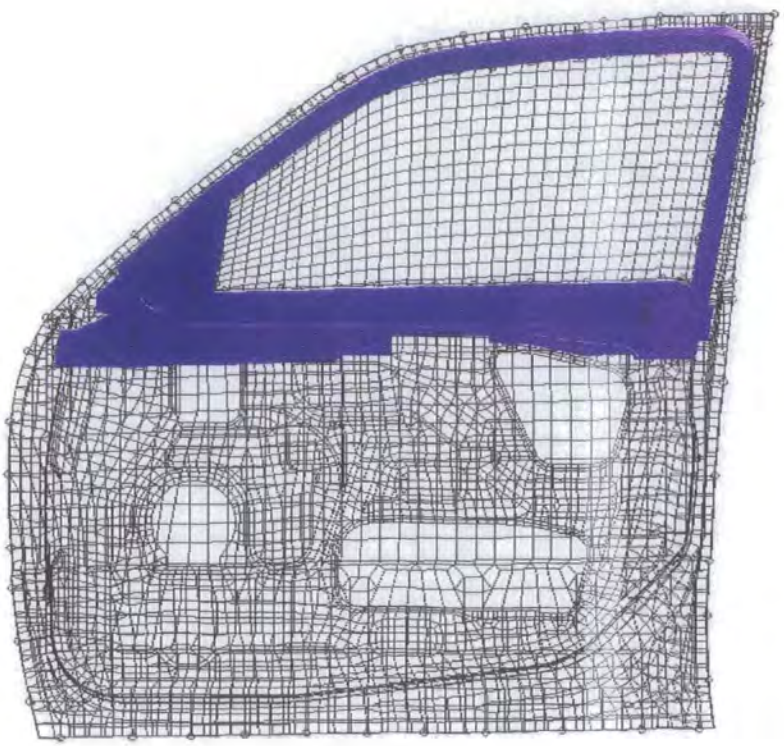

Figure 6-4. Model 1 (original model)

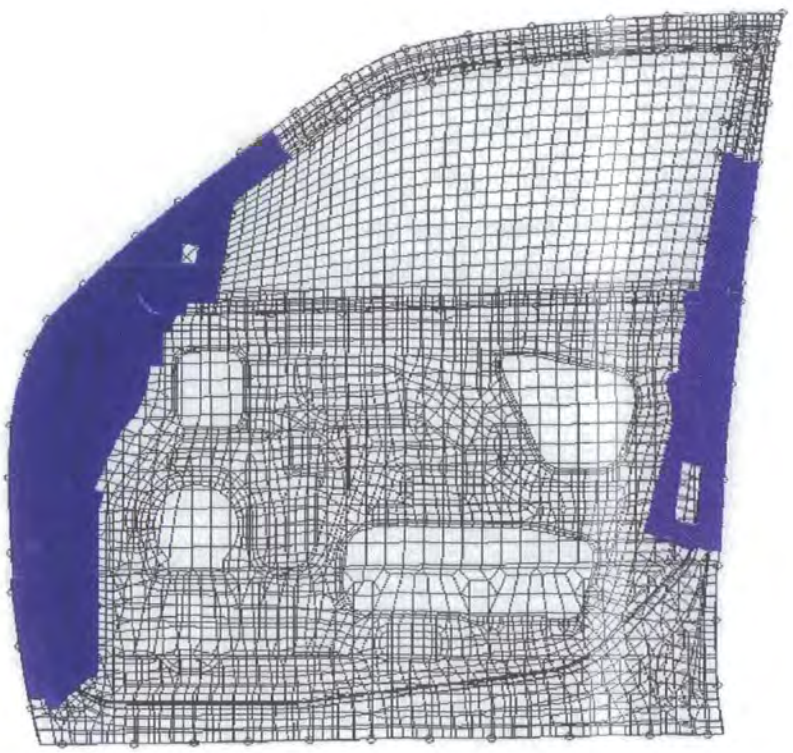

Figure 6-5. Model 3 (reinforcement 1)

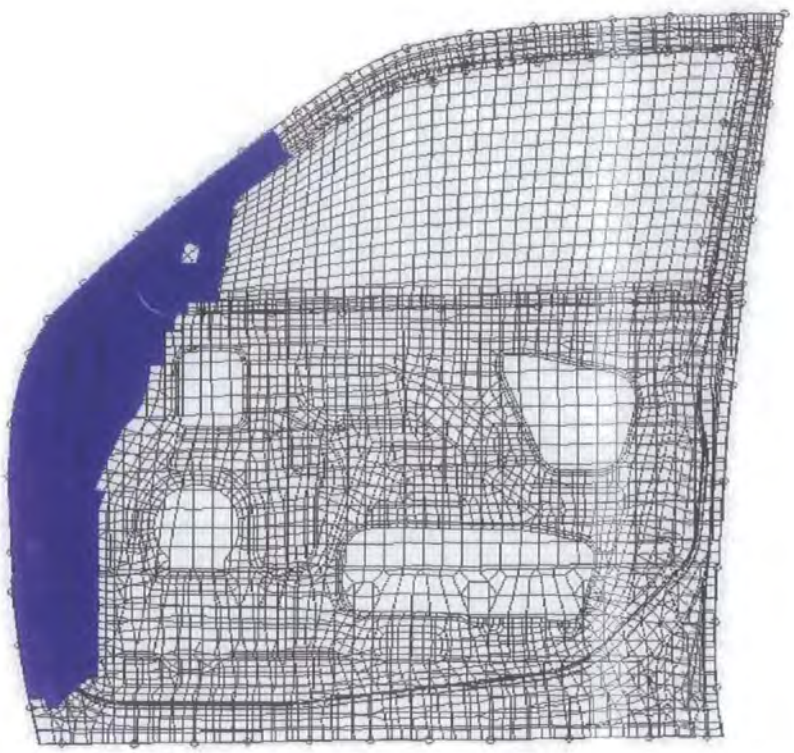

Figure 6-6. Model 4 (reinforcement 2)

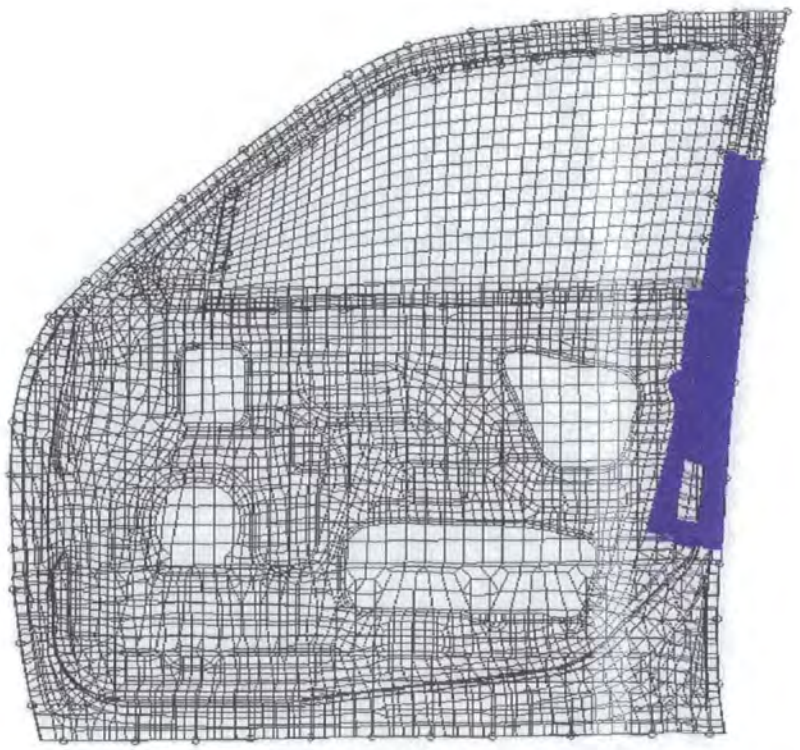

Figure 6-7. Model 5 (reinforcement 3)

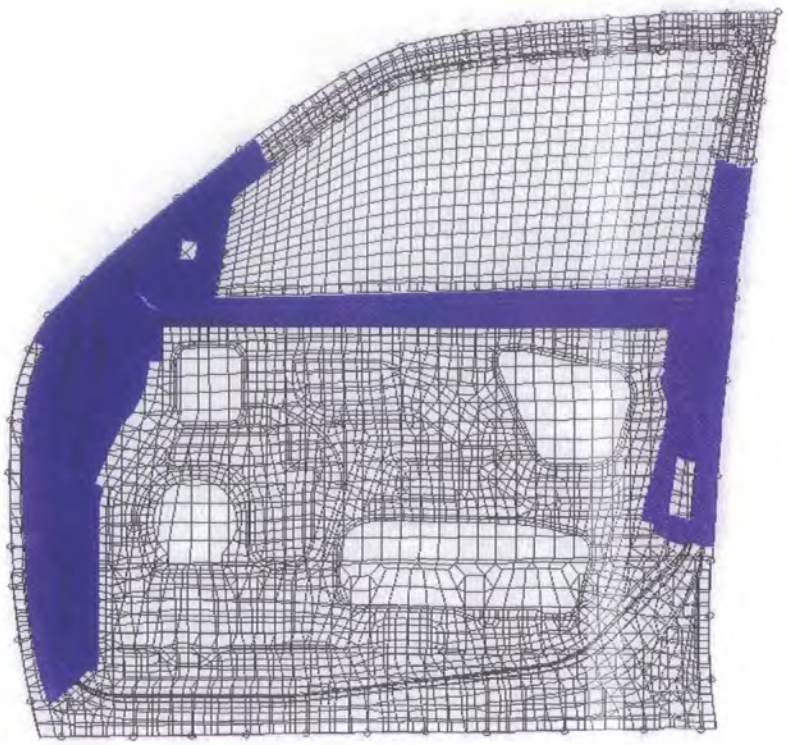

Figure 6-8. Model 6 (reinforcement 4)

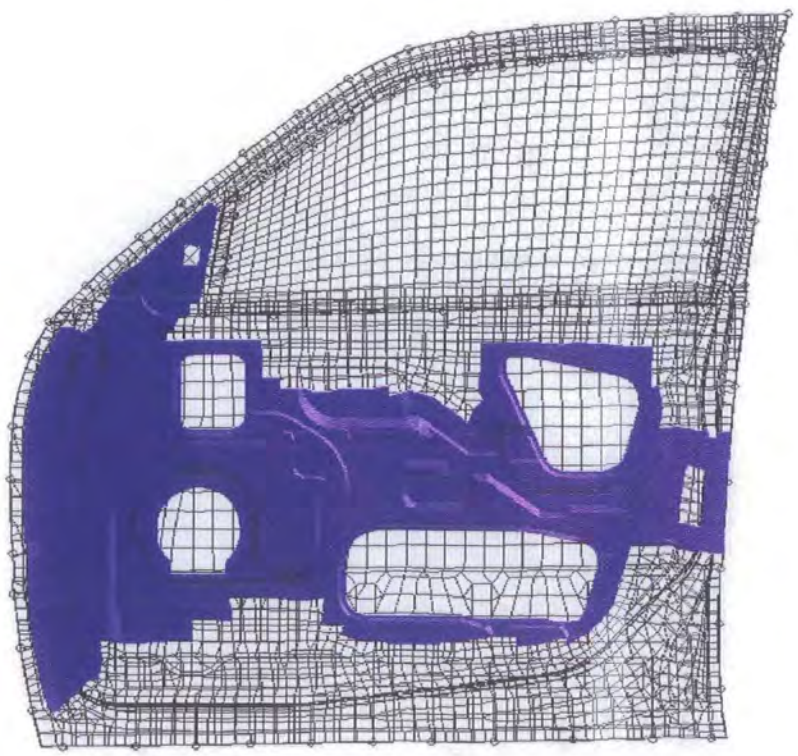

Figure 6-9. Model 7 (reinforcement 5)

Figure 6-10. Model 8 (reinforcement 6)

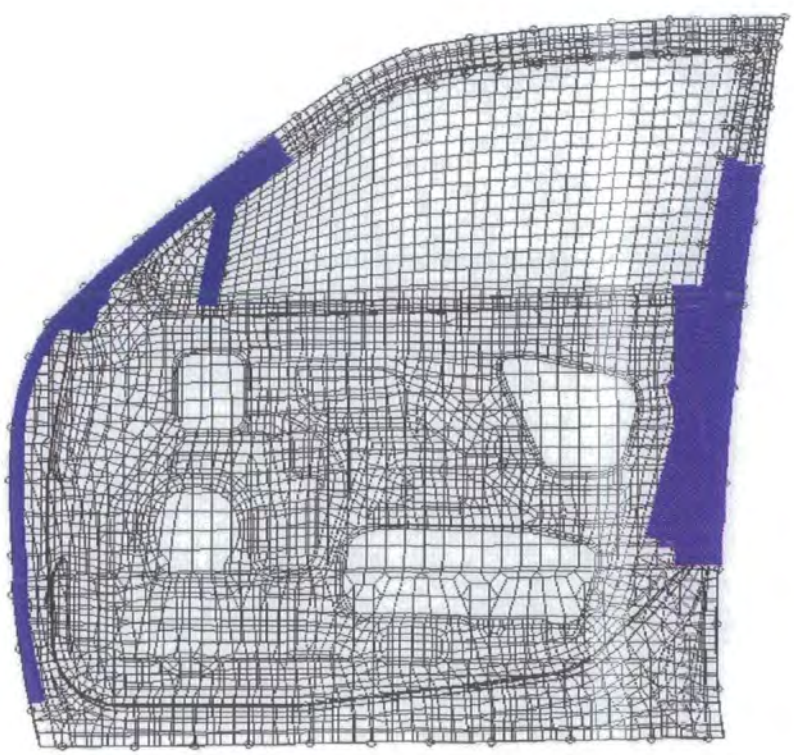

Figure 6-11. Model 9 (Reinforcement 7)

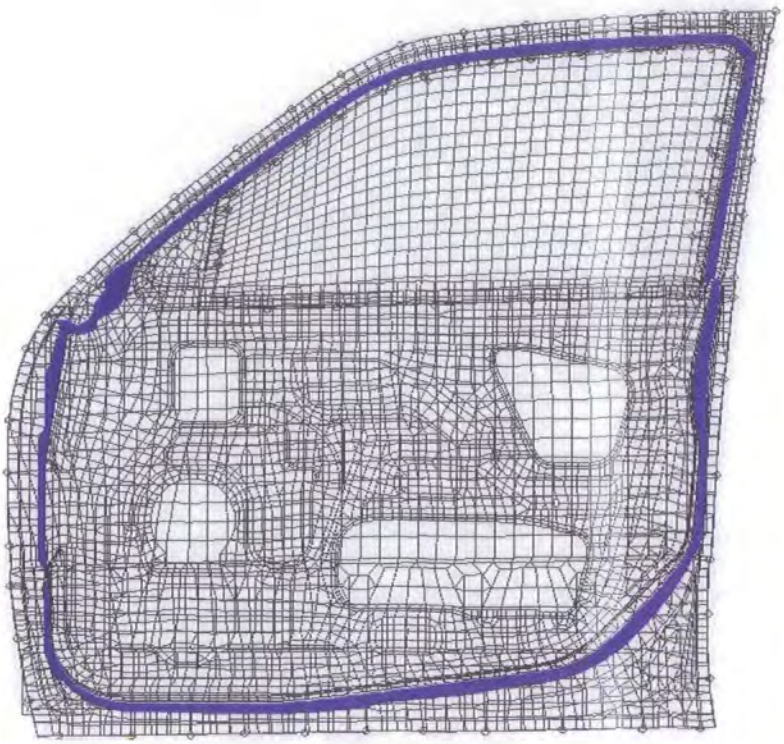

Figure 6-12. Model 10 (reinforcement 8)

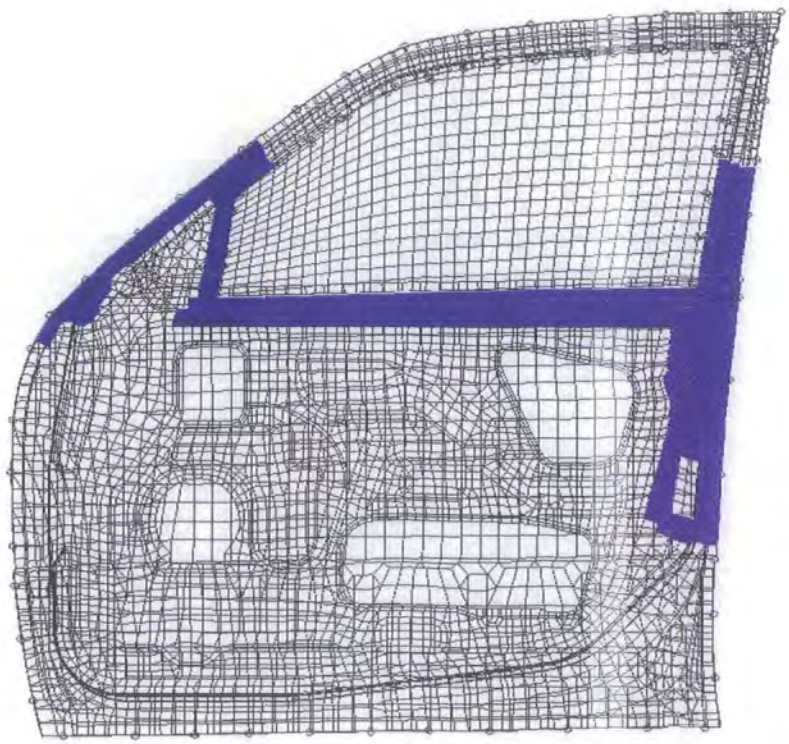

Figure 6-13. Model 11 (reinforcement 9)

6.2. Analysis

The load and displacement boundary conditions are as follows :

1. The load of air pressure acting as a distributed load applied to the whole area of the outer panel and glass, and its direction is normal to the panel and glass elements as shown in figure 6-14.
2. Two points of door hinge mounting on A-pillar region and one point of door latch mounting on B-pillar region are fixed. (Figure 6-15)
3. The loading is assumed to be of sinusoidal form and is applied at the first three natural frequencies for each model. It is assumed that the worst case for vibrational deformation of the door panel will be at a forcing frequency which coincides with one of the structural natural frequencies.

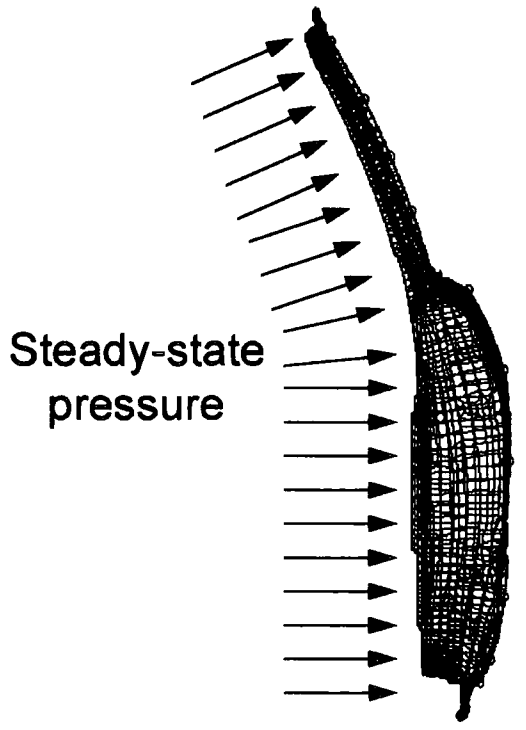

Figure 6-14. Boundary condition of models (pressure loading)

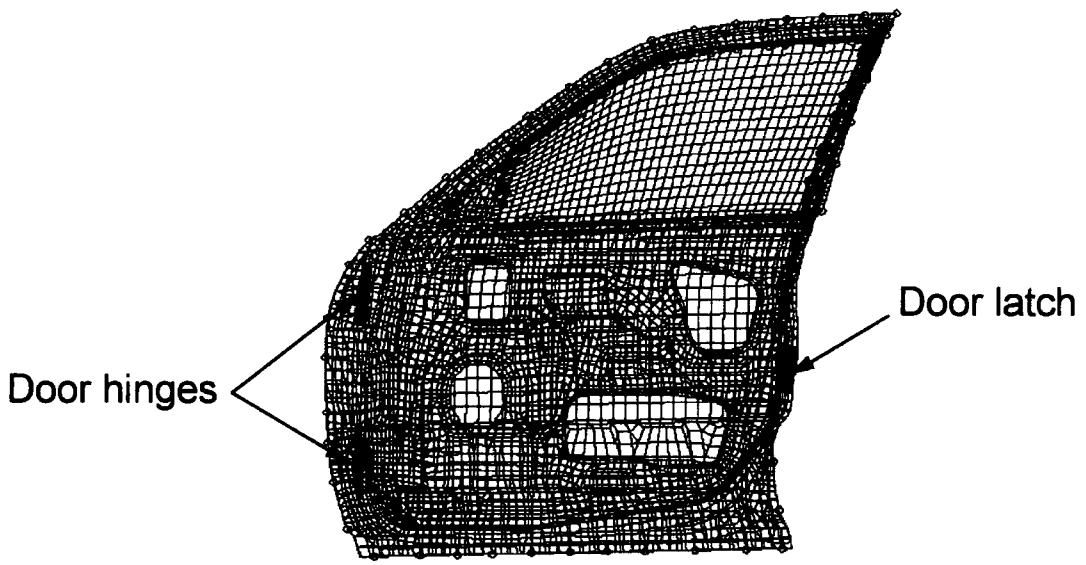

Figure 6-15. Boundary condition of models (fixed area)

Stress distributions and nodal displacements of several reinforcing configurations have been obtained by ABAQUS and graphs of the deformations built up.

The first two or three modes of vibration are used as a basis for the dynamic stiffness analysis because generally the maximum deformation of the frame occurs in the first or second mode. It will be seen that the fourth and higher modes have much smaller amplitudes under forced vibration of the car door. (Table 7-3)

Maximum stresses and displacements of the modes will be compared with each other.

The values of Young's modulus, density, and Poisson ratio for steel and glass are shown on table 6-3.

Value (unit)	Steel	Glass
Young's modulus (kg/mm·sec^2)	2.068×10^8	6.5×10^7
Density (kg/mm^3)	7.827×10^{-6}	2.334×10^{-6}
Poisson ratio	0.3	0.183

Table 6-3. Engineering values of steel and glass[40]

(In this thesis, units kg/mm·sec^2 and kg/mm^3 are used instead of the standard units Pa (kg/m·sec^2) and kg/m^3 because the door panel is designed by the mm length unit.)

7. Results and Discussion

7.1. Results

Figures 7-1 to 7-9 show the contours of displacement and the deformed shapes (which are amplified by a factor of 20) of model 1 under forced vibration at each natural frequency.

Figures 7-10 to 7-23 present the displacement contours of each model under forced vibration at the natural frequency where the maximum displacement occurs (see table 7-2). For contour figures, the largest deformation occurs in the red zone. The direction of the displacements which are shown in contour figures is Y-direction of the absolute coordinate system. For clarity, no contour scale is included in these figures, which are intended to show the form of the displacement. Table 7-1 shows the maximum displacement value for each model.

Figure 7-20 and 7-21 are obtained by changing the thickness of reinforcement 9 (model 11) to 1.5mm and 2.0mm each, and figure 7-22 is the result of the more detailed model which is generated from model 1.

Figure 7-23 shows the displacement contour of model 2 with sealing system. (It is same as figure 7-10, see section 7.2 table 7-5)

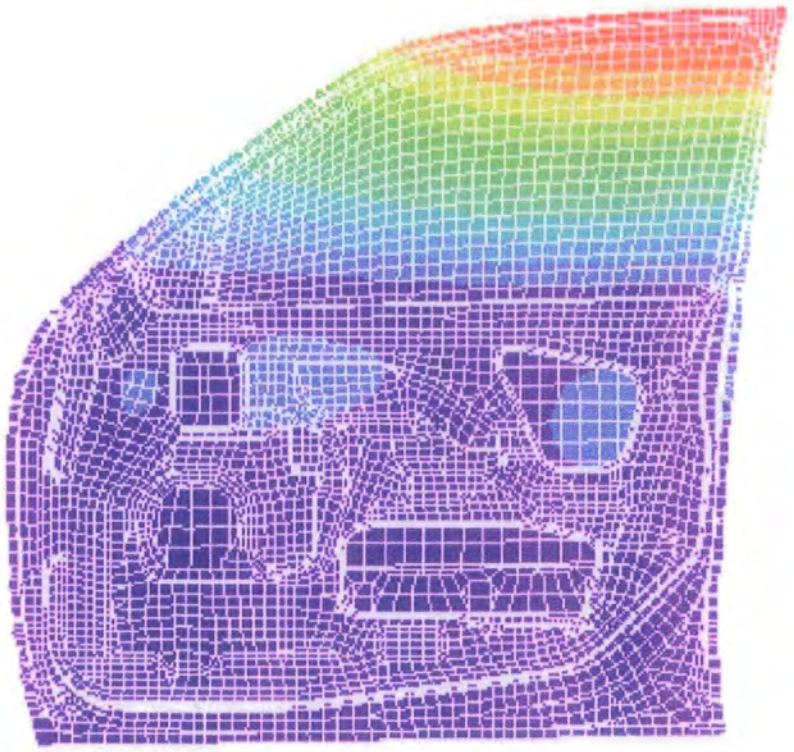

Figure 7-1. Displacement contour of model 1 at the 1st natural frequency

Figure 7-2. Deformation quarter view of model 1 at the 1st natural frequency

Figure 7-3. Deformation rear view of model 1 at the 1st natural frequency

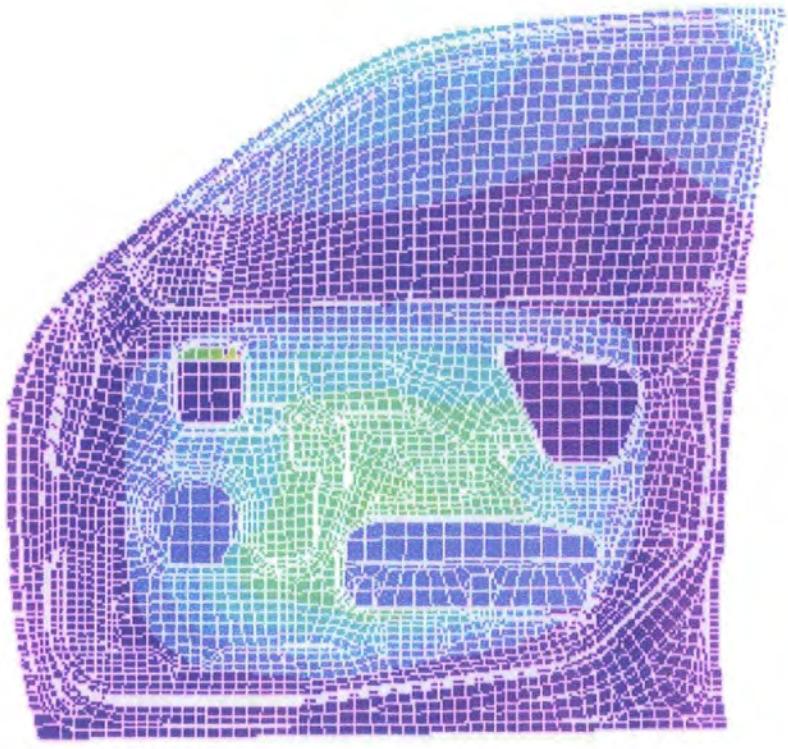

Figure 7-4. Displacement contour of model 1 at the 2nd natural frequency

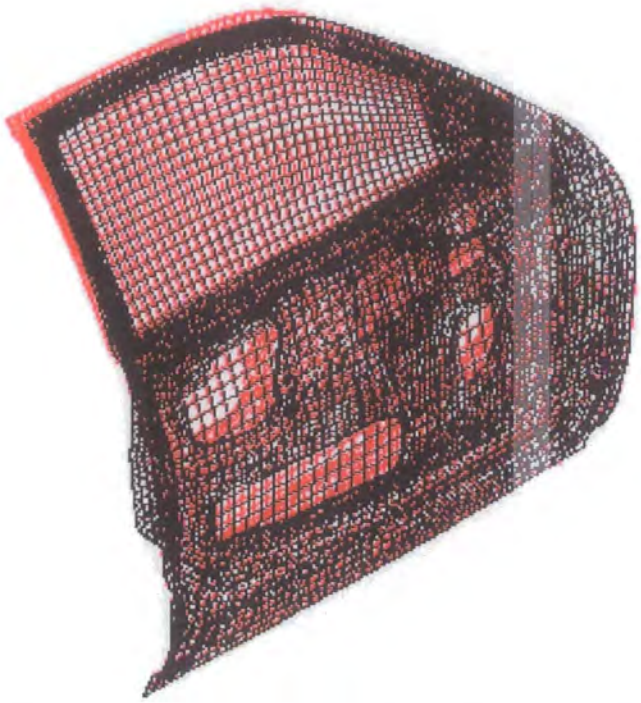

Figure 7-5. Deformation quarter view of model 1 at the 2nd natural frequency

Figure 7-6. Deformation rear view of model 1 at the 2nd natural frequency

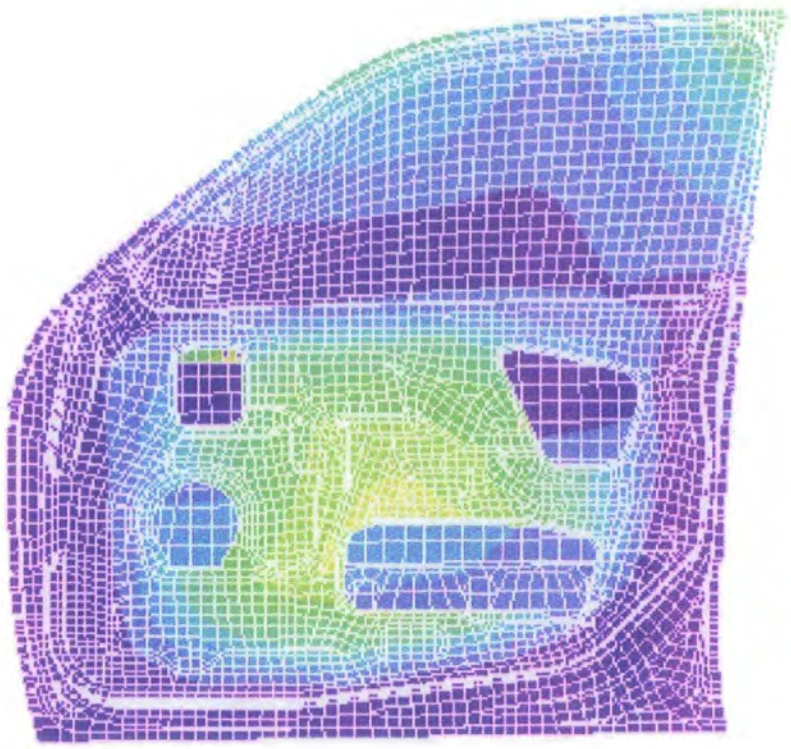

Figure 7-7. Displacement contour of model 1 at the 3rd natural frequency

Figure 7-8. Deformation quarter view of model 1 at the 3rd natural frequency

Figure 7-9. Deformation rear view of model 1 at the 3rd natural frequency

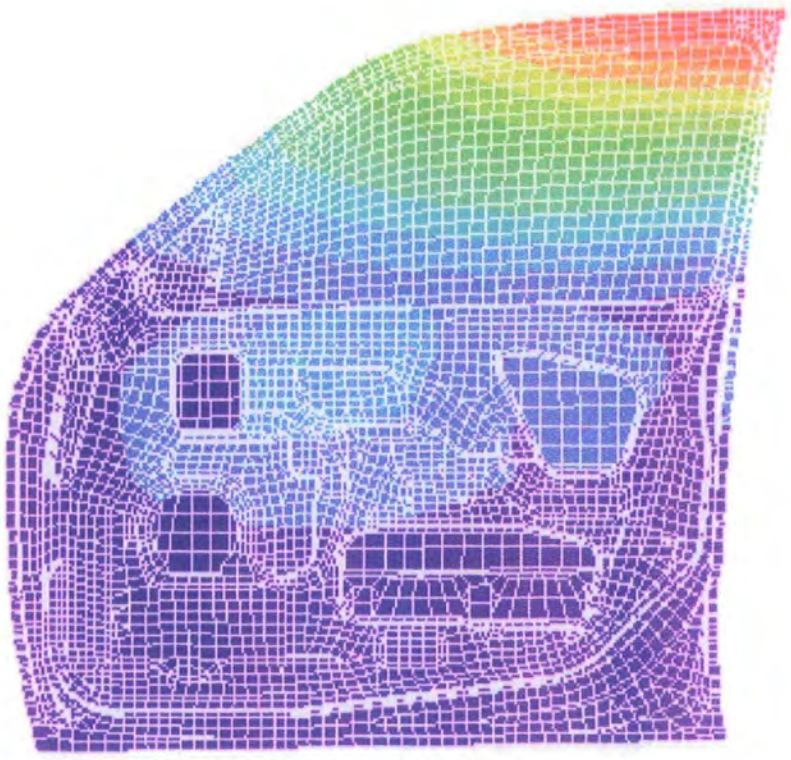

Figure 7-10. Displacement contour of model 2

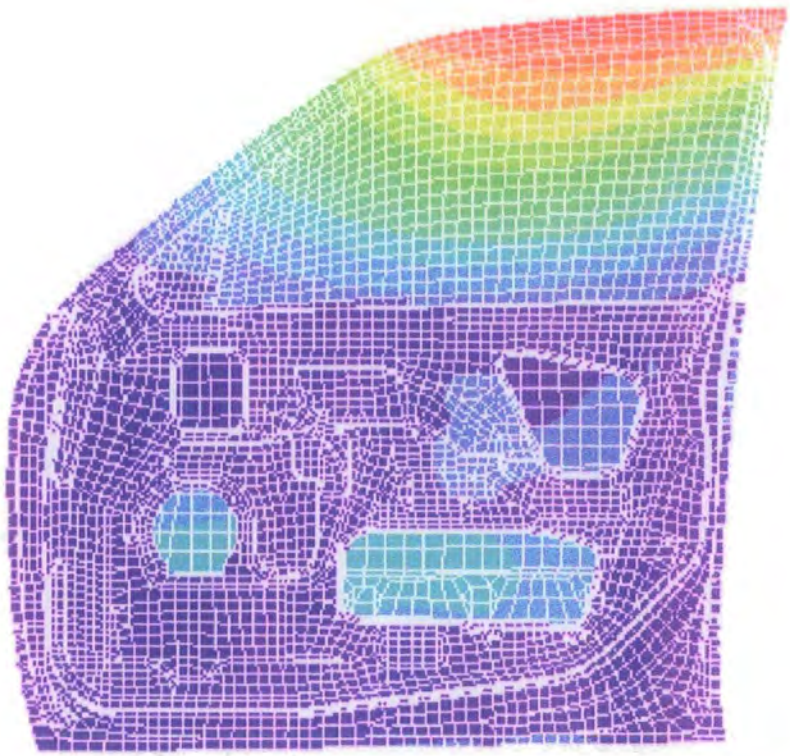

Figure 7-11. Displacement contour of model 3

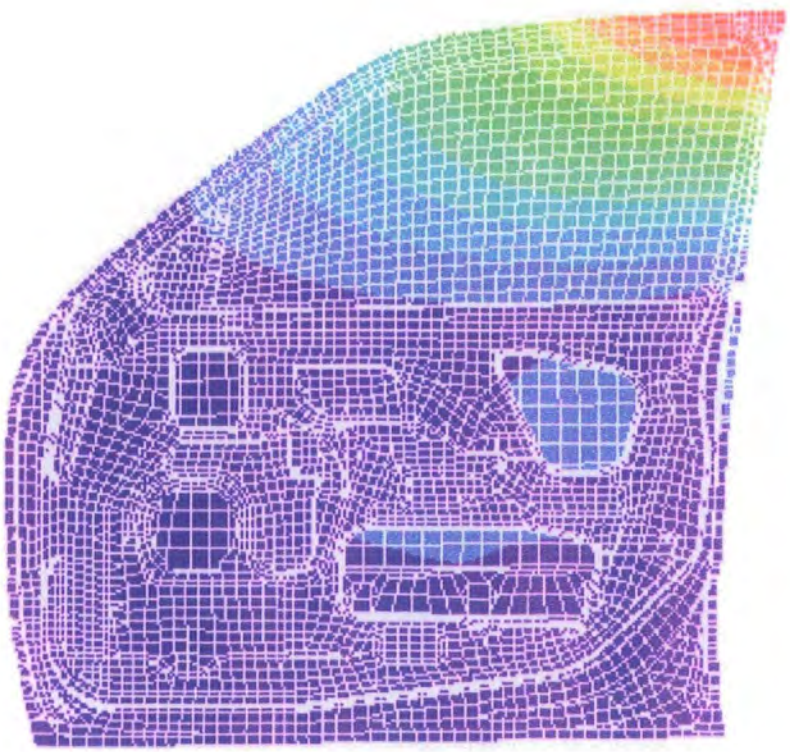

Figure 7-12. Displacement contour of model 4

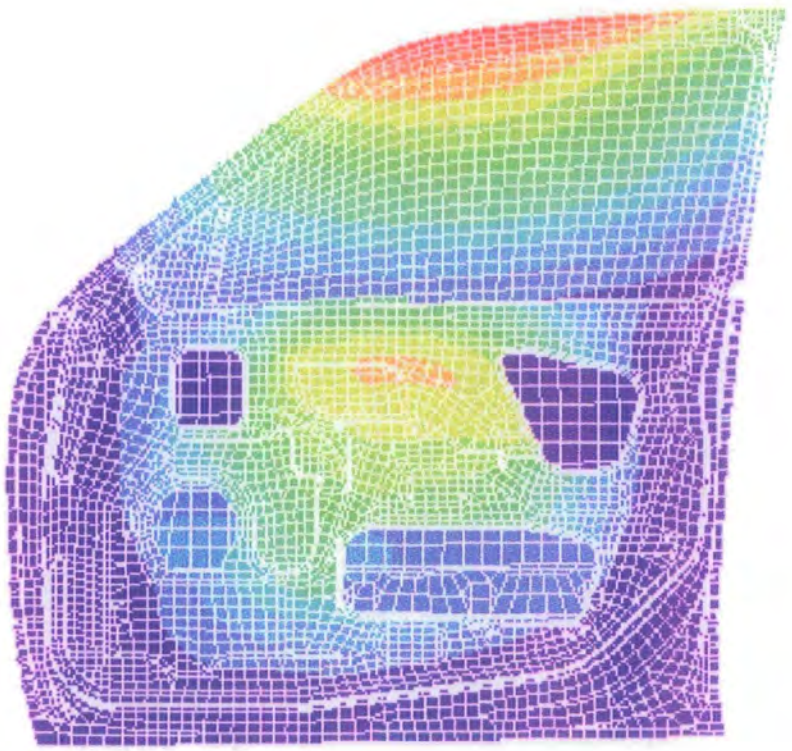

Figure 7-13. Displacement contour of model 5

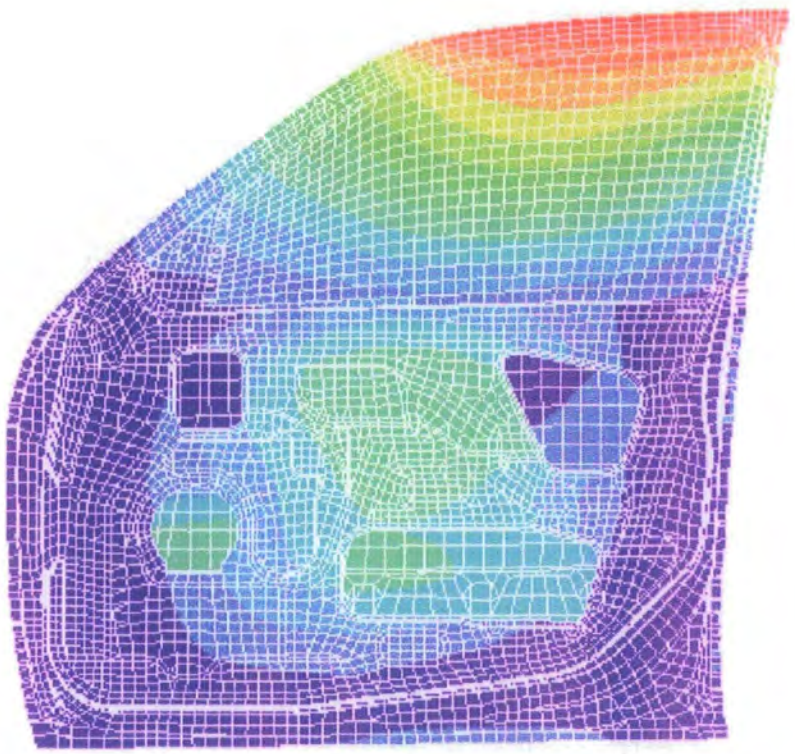

Figure 7-14. Displacement contour of model 6

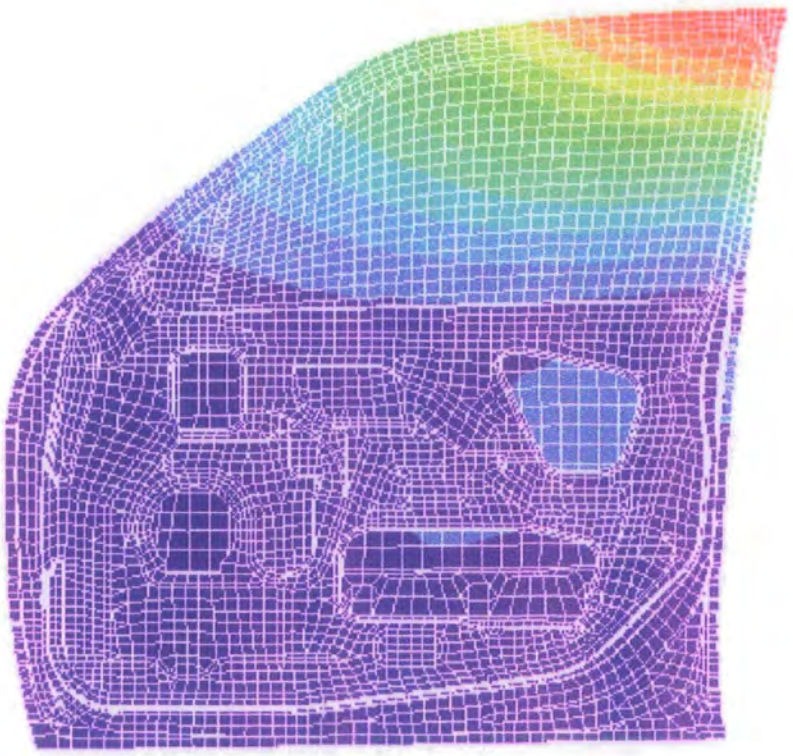

Figure 7-15. Displacement contour of model 7

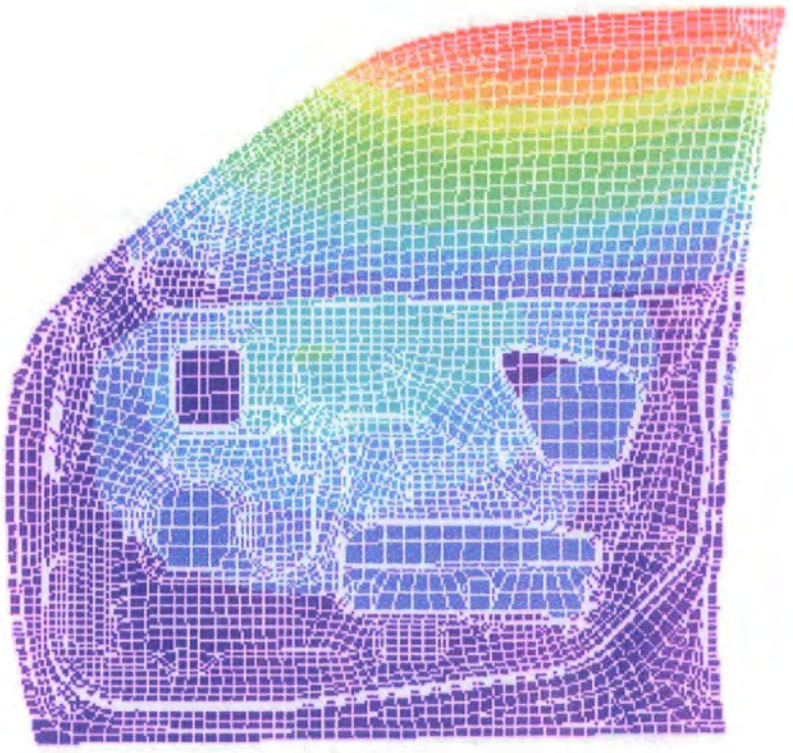

Figure 7-16. Displacement contour of model 8

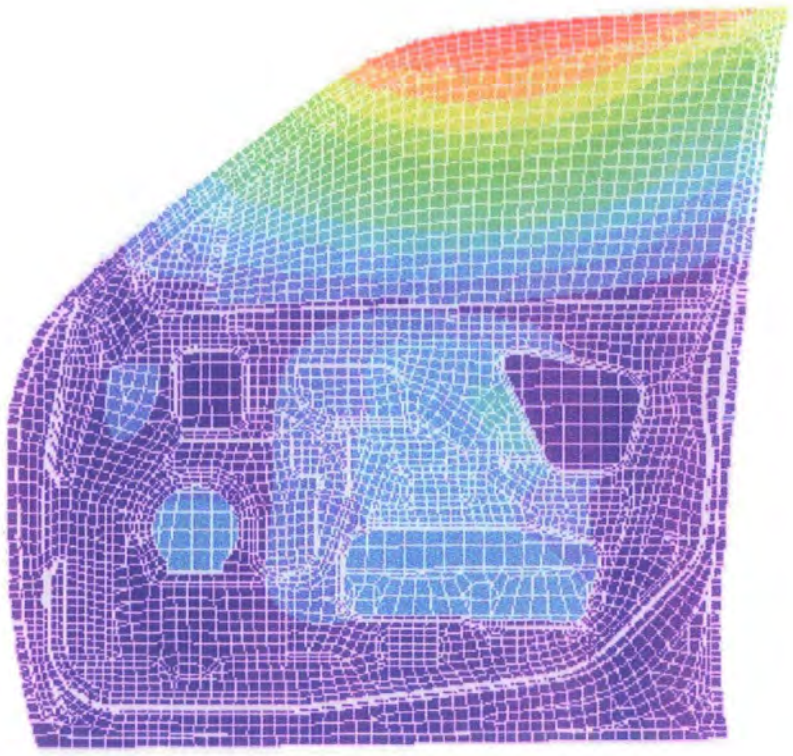

Figure 7-17. Displacement contour of model 9

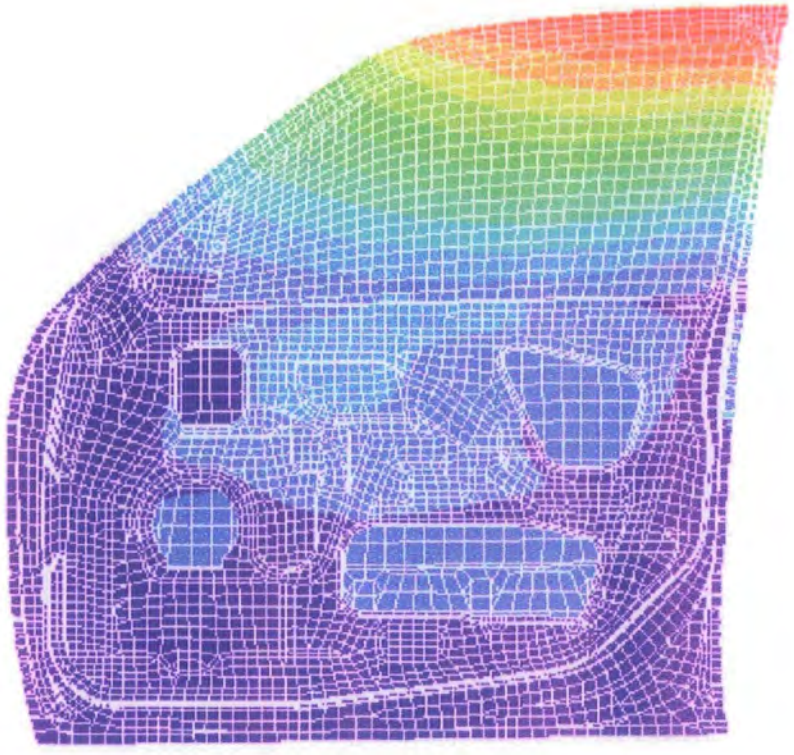

Figure 7-18. Displacement contour of model 10

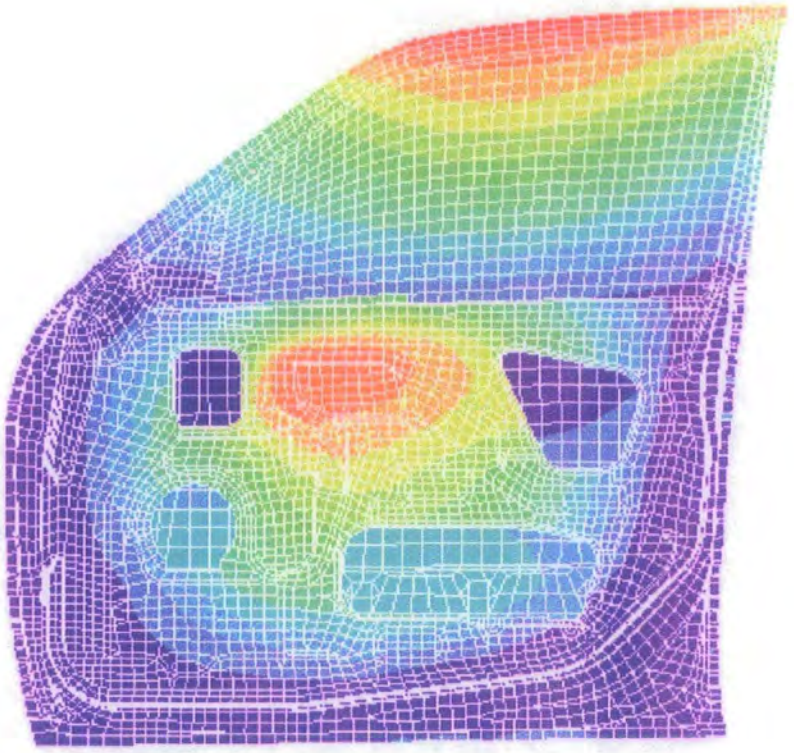

Figure 7-19. Displacement contour of model 11

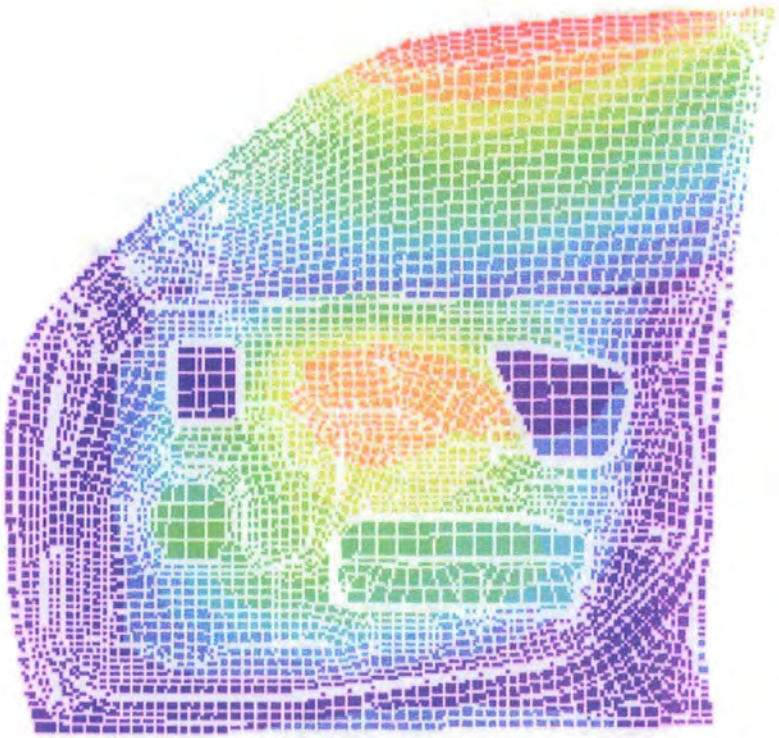

Figure 7-20. Displacement contour of model 12

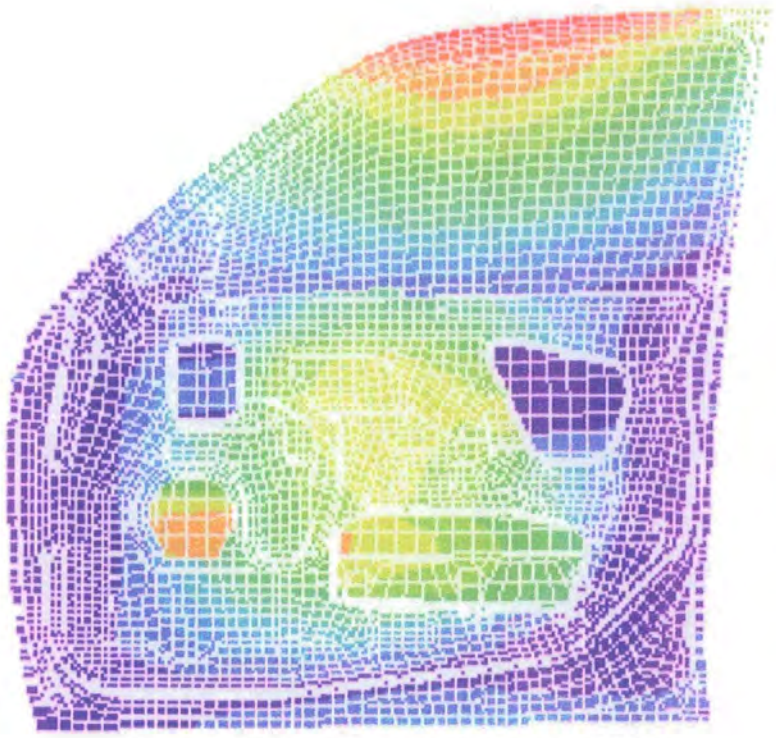

Figure 7-21. Displacement contour of model 13

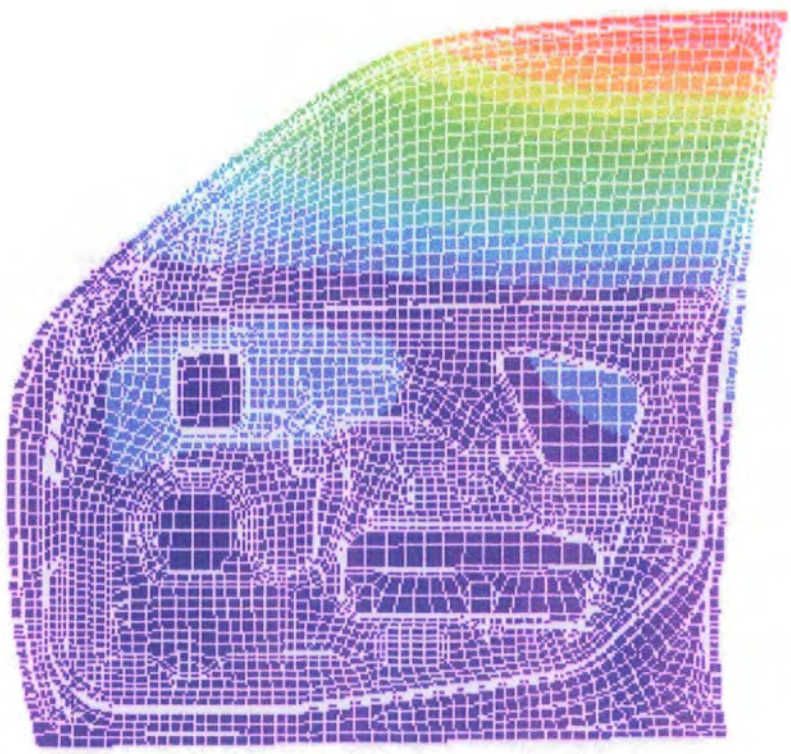

Figure 7-22. Displacement contour of more detailed model

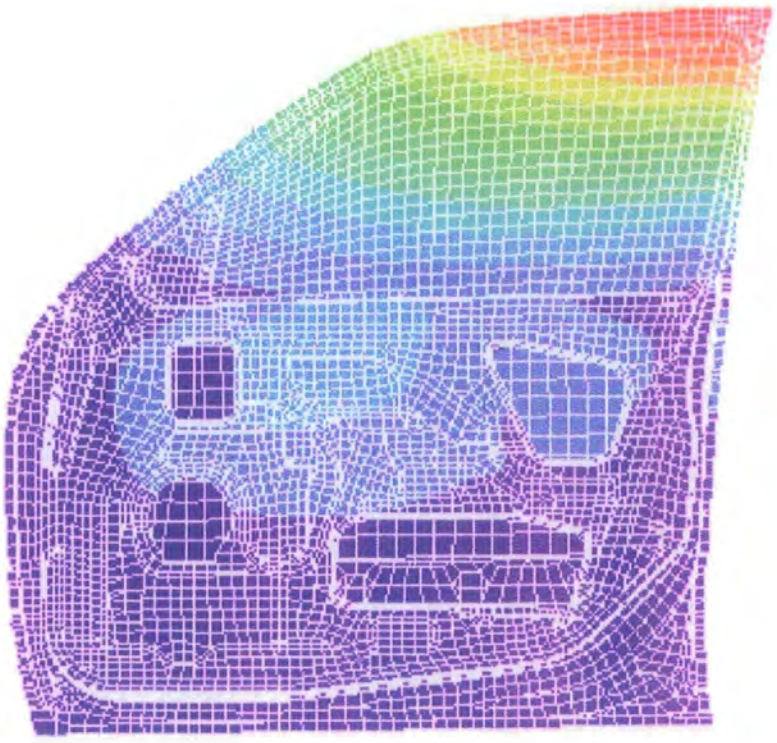

Figure 7-23. Displacement contour of model 2 with sealing system

The relationship between maximum displacements and maximum stresses is presented on table 7-1. The smallest maximum displacement is occurred on model 11 which has the smallest value of the maximum stress.

Model	Eigenmode	Max. displacement (mm)	Max. stress (kg/mm·sec²)
1	1	6.171	3.6076E+05
2	1	7.498	4.0607E+05
3	2	3.298	1.6200E+05
4	1	7.145	3.8792E+05
5	2	3.397	1.2430E+05
6	2	2.991	1.4865E+05
7	1	6.863	3.9130E+05
8	1	3.287	1.8794E+05
9	2	3.227	1.4073E+05
10	1	4.771	3.5357E+05
11	1	2.525	1.0428E+05

Table 7-1. Max. displacements and stresses of models

The maximum displacements and the natural frequencies of each model are listed in table 7-2.

Model	Eigenmodes	Natural frequency (Hz)	Max. displacement (mm)
1	Eigenmode 1	24.3	6.171
	Eigenmode 2	42.2	1.541
	Eigenmode 3	43.6	1.103
2	Eigenmode 1	25.6	7.498
	Eigenmode 2	30.2	1.571
	Eigenmode 3	44.5	3.562
3	Eigenmode 1	35.2	1.229
	Eigenmode 2	39.3	3.298
	Eigenmode 3	47.4	3.02
4	Eigenmode 1	28.6	7.145
	Eigenmode 2	33.0	1.735
	Eigenmode 3	45.7	3.37
5	Eigenmode 1	31.4	3.013
	Eigenmode 2	33.6	3.397
	Eigenmode 3	46.0	3.484
6	Eigenmode 1	38.9	2.638
	Eigenmode 2	40.1	2.991
	Eigenmode 3	46.6	3.12
7	Eigenmode 1	28.2	6.863
	Eigenmode 2	33.7	1.31
	Eigenmode 3	45.6	3.474
8	Eigenmode 1	32.1	3.287
	Eigenmode 2	37.4	0.821
	Eigenmode 3	48.8	3.094
9	Eigenmode 1	33.2	1.011
	Eigenmode 2	38.3	3.227
	Eigenmode 3	47.7	3.191
10	Eigenmode 1	28.8	4.771
	Eigenmode 2	31.5	1.892
	Eigenmode 3	45.7	3.453
11	Eigenmode 1	35.6	2.525
	Eigenmode 2	38.3	2.26
	Eigenmode 3	46.1	3.339
12	Eigenmode 1	37.1	2.12
	Eigenmode 2	40.1	2.237
	Eigenmode 3	46.3	3.293
13	Eigenmode 1	39.3	1.711
	Eigenmode 2	42.8	2.166
	Eigenmode 3	46.4	3.186

Table 7-2. Details of natural frequencies and max. displacements of models

7.2. Discussion

Although the values of maximum displacement in table 7-2 seem high in comparison with our experience of door panel vibration, it should be recognised that they result from an extreme case, i.e. steady state forcing at a natural frequency causing a condition of resonance. In practice, this type of forcing is likely to occur for only a fraction of a second, causing displacements to be much smaller.

Table 7-3 shows the displacements of the first ten vibration modes of model 11. The displacements of the fourth and higher modes are much smaller than the displacements of the first three modes. In addition, according to equation (3.2.5), when the car speed is 100km/h, the vortex shedding frequency in the outside mirror area is around 40Hz. Table 7-3 shows this to be in the range of the first three modes. For these two reasons, it is justifiable to use the first three modes for analysis of pressures oscillating as a result of air flow past a wing mirror.

Eigenmode	Natural frequency (Hz)	Max. displacement (mm)
1	35.6	2.513
2	38.3	2.270
3	46.1	3.320
4	54.3	0.7041
5	56.2	0.6251
6	64.1	0.6462
7	67.0	0.9606
8	77.3	0.2479
9	82.7	0.1638
10	83.8	0.1533

Table 7-3. Max. displacements under forced vibration at the first 10 natural frequencies for model 11

There are many parts below the door belt region in an actual vehicle, such as the side impact safety beam and the window glass regulator, which have not been included in the finite element model in this study. However, for one model a more detailed finite element study including these features has been run. Table 7-4 shows that the first two natural frequencies remained similar while some 10% change in the third natural frequency was observed. Since the model shapes were similar with and without these features, and assuming that the effects on displacements by neglecting these features will be the same for all models, the choice of an optimum design from the reduced set of models should remain valid.

Model	Eigenmodes	Natural frequency (Hz)
1	Eigenmode 1	24.3
	Eigenmode 2	42.2
	Eigenmode 3	43.6
More detailed model	Eigenmode 1	24.4
	Eigenmode 2	43.6
	Eigenmode 3	48.1

Table 7-4. Comparison model 1 (original model) with more detailed model

However, as can be seen from table 7-2, some models exhibit a maximum deformation when forced at the third natural frequency. In cases such as these the maximum deformation occurs in the below door belt region because of the characteristic form of the third mode shape. The study of the more detailed models has shown that these displacements are substantially overpredicted by the simplified models, and that when the structures such as the side impact safety beam are included the deformation is much reduced. For this reason,

the author has neglected any maximum displacements occurring when forced at the third natural frequency.

The boundary conditions for the analysis included no consideration of the door seal. The sealing system provides some increased stiffness against vibrational deformation, but the influence is very small in comparison with the stiffness of the door panel. Thus the sealing system was omitted from the model. In verification, table 7-5 presents the finite element results which show no difference between the model 2 without a sealing system and the model with a sealing system.

Model	Eigenmodes	Natural frequency (Hz)	Max. displacement (mm)
2	Eigenmode 1	25.6	7.498
	Eigenmode 2	30.2	1.571
	Eigenmode 3	44.5	3.562
Model with sealing system	Eigenmode 1	25.6	7.498
	Eigenmode 2	30.2	1.571
	Eigenmode 3	44.5	3.562

Table 7-5. Analysis of model 2 (base model) about sealing system

There is another variable to be considered which is called 'glass-run', representing the fixture running the glass along the frame, but the glass can be fixed to the frame tightly by the glass-run, constraining the glass against rotation relative to the frame. It is therefore reasonable to use a fixed type MPC to represent the glass fixing to the frame.

By modifying the reinforcements of the door panel the displacement of the door frame due to dynamic pressure is found to change, though different designs cause different results.

Table 7-6 and figure 7-24 show the maximum displacements and weights of the models. From models 3, 4, and 5, it can be found that the effect of the B-pillar reinforcement is much greater than that of the A-pillar reinforcement.

It is also clear from figure 7-24 that there is an underlying reciprocal relationship between the weight of the door panel and its maximum displacement response. However, the relationship is not a simple one.

The choice of quantitative criteria for selection of an optimum from the thirteen models is also a difficult problem. Moreover, different manufacturers will apply different criteria based on the market position of their vehicles. For example, a low volume of production luxury car might have model 13 as an optimum, whereas a high volume inexpensive car might have model 2 as an optimum. These are extreme cases, and a more balanced engineering approach would look for a reasonably low displacement in combination with a reasonably low weight. In view of this model 11 seems a more educated choice of an optimum for most vehicles. This design weighs almost 1kg less than the original (model 1), and has a maximum displacement of 2.525mm which compares very favourably with the original 6.171mm. In addition, the maximum stress has been reduced by a factor of 3.5, giving extra benefits in durability and fatigue resistance.

Model	Max. displacement (mm)	Eigenmode	Natural frequency (Hz)	Weight (kg)
1	6.171	1	24.3	18.495
2	7.498	1	25.6	15.901
3	3.298	2	39.3	18.488
4	7.145	1	28.6	17.591
5	3.397	2	33.6	16.761
6	2.991	2	40.1	18.884
7	6.863	1	28.2	18.162
8	3.287	1	32.1	21.062
9	3.227	2	38.3	17.777
10	4.771	1	28.8	17.686
11	2.525	1	35.6	17.532
12	2.237	2	40.1	17.95
13	2.166	2	42.8	18.648

Table 7-6. Max. displacements and weights of models

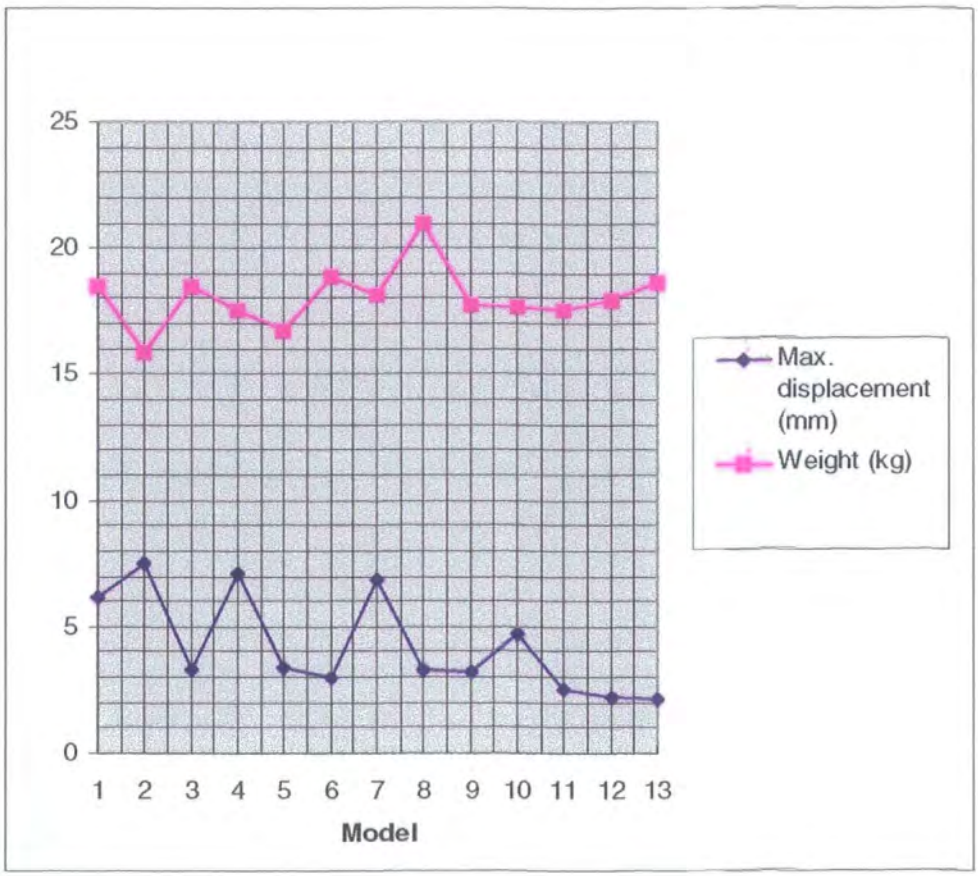

Figure 7-24. Graph for the max. displacements and weights of models

The reduction in displacement from 6.171mm to 2.525mm amplitude has a further, major significance in the reduction of aspiration wind noise. This results from the door seal design, a schematic cross-section of which is shown in figure 7-25. When the door is opened, the seal is of approximately circular cross section, but it compresses by an amount β (as shown on the right hand side of the figure) when the door is closed. In a typical vehicle door seal, the distance of compression β is chosen to be around 4 or 5mm. Thus the reduction of door vibration to a value below this may be seen to have a very substantial effect in noise reduction.

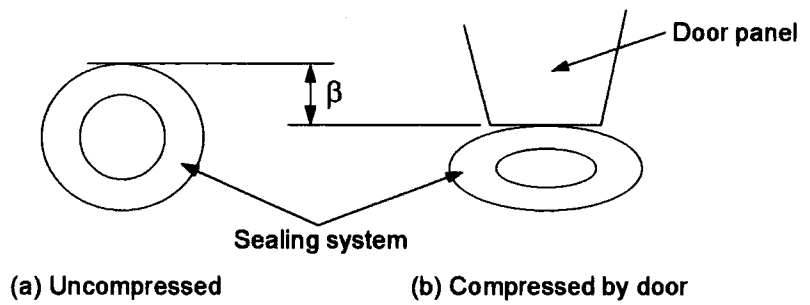

Figure 7-25. Compression of sealing system

8. Conclusions and Recommendations for Further Work

A number of different designs for car door panel reinforcements have been assessed, using the finite element method, for dynamic stiffness performance and weight. This gives valuable information on the cost of bringing about reductions in wind noise.

It is found to be more weight-effective to reduce the bending vibration displacement by reinforcing not the whole frame area but only the frame side regions. So if the frame reinforcement and outer rail are removed, and small reinforcements are added to only the B-pillar and A-pillar areas of the inner and outer panels, both weight reduction and increased stiffness may be achieved.

It has further been found that the effect of the B-pillar reinforcement is much greater than that of A-pillar reinforcement.

The door frame vibration may in general be reduced by increasing the reinforcements of the door frame side. But it is recognised that overweight brings some negative effects with respect to the cost and emissions.

The design of a vehicle's door panel assembly is a complex process which should be considered from the production of the unit on line. The engineering designer aims to reduce the weight and the cost of vehicles, because the final aim of all those processes is creation of profits. Thus the improvements in wind noise performance must be considered in relation to the cost of bringing

them about. This research suggests a cost-effective optimum design (see figure 6-13 on page 69) to cut the displacement of bending vibration to 40% of the original while at the same time reducing the weight by almost 1kg. In addition, the maximum stress has been reduced by a factor of 3.5, giving extra benefits in durability and fatigue resistance. In order to achieve more noise reduction, increasing the weight and the cost may be required, and the modifications may cause many difficulties in line processes.

In the future, by using a super computer, it will be possible to model and analyse not only the door panel assembly but also the more detailed features of the door including trims, mouldings, and sealing systems. Moreover engineers will be able to obtain the relationship between the overlap magnitude of the sealing system and the stiffness of the door panel assembly for many possible cases. They can use this information to design the door panel assembly and the sealing system optimally, decreasing the aspiration wind noise significantly. Taking a step forward, there can also be structural resonant vibration in panels such as the quarter outer panel, and it is possible to reduce the resulting noise by similar techniques.

In addition, a fully coupled analysis which includes aerodynamics, structural vibration, and interior acoustics problem will be made possible.

References

1. R. H. Barnard, *Road Vehicle Aerodynamic Design : An Introduction*, Addison Wesley Longman Limited, London, 1996.
2. *Test Report* : Door Stiffness, HMC Engineering Research Centre, 1991, 1994, 1995.
3. *Stiffness Analysis of Vehicle Door Frame*, HMC Engineering Research Centre, 1997.
4. Larry J. Segerlind, *Applied Finite Element Analysis*, John Wiley & Sons, Inc., U.S.A, 1976.
5. *Introduction to ABAQUS/Standard*, Hibbitt, Karlsson & Sorenson Inc., 1995.
6. *Getting Started with ABAQUS/Standard*, Hibbitt, Karlsson & Sorenson Inc., U.S.A, 1994.
7. *ABAQUS User's Manual Volume 1;2;3*, Hibbitt, Karlsson & Sorenson Inc., 1994.
8. *ABAQUS/Post Manual*, Hibbitt, Karlsson & Sorenson Inc., U.S.A, 1994.
9. *ABAQUS/Standard Example Problems Manual Volume 1;2*, Hibbitt, Karlsson & Sorenson Inc., U.S.A, 1994.
10. *Engineering Specification* : Door Complete Assembly, HMC Passenger Car Body Engineering Team, 1993.
11. "Passenger Car Door System Crush Test Procedure", *SAE (Society of Automotive Engineers, Inc.) J367 JUN80*, U.S.A, 1981.

12. "Vehicle Passenger Door Hinge Systems", *SAE J934a*, U.S.A, 1981.

13. "Passenger Car Side Door Latch Systems", *SAE J839b*, U.S.A, 1981.

14. "Sound Level for Passenger Cars and Light Trucks", *SAE J986b*, U.S.A, 1981.

15. "Maximum Sound Level for Passenger Cars and Light Trucks", *SAE J1030*, 1981.

16. Ferdinand P. Beer, and E. Russell Johnston Jr., *Mechanics of Materials* (Korean edition), Cheong - Mun - Kak, Seoul, 1986.

17. T.Y. Yang, *Introduction of Finite Element Structural Analysis* (Korean edition), Scientific Technology Publications, Inc., Seoul, 1997.

18. Ray. E. Bolz, and George L. Tuve, *Handbook of tables for Applied Engineering Science* : 2nd Edition, CRC Press, U.S.A, 1973.

19. B. S. Massey, *Mechanics of Fluids* : 6th edition, Chapman and Hall Ltd., London, 1989.

20. J. P. Howell, "The Side Load Distribution on a Rover 800 Saloon Car under Crosswind Conditions", *Proceedings* 2nd Wind Engineering Society Conference, Rover Group, Warwick, 1994.

21. M. Docton, *The Simulation of Transient Cross Winds on Passenger Vehicles*, Durham University, 1996.

22. M. Docton, *Numerical Predictions of a Flow Around a Simple Vehicle Form Under the Influence of a Transient Cross-Wind Gust*, Durham University, 1996.

23. Roger A. Anderson, *Fundamentals of Vibrations*, The Macmillan Company, U.S.A, 1967.

24. C. F. Beards, *Structural Vibration Analysis : Modelling, Analysis and Damping of Vibrating Structures*, Ellis Horwood Series in Engineering Science, Ellis Horwood Ltd, Chichester, 1983.

25. L. F. Boswell, and C. D'Mello, *Dynamics of Structural Systems*, Blackwell Scientific Publications, Inc., Oxford, 1993.

26. Frank Fahy, *Sound and Structural Vibration : Radiation, Transmission and Response*, Academic Press Inc. (London) Ltd., London, 1985.

27. D. J. Hatter, *Matrix Computer Methods of Vibration Analysis*, Butterworths & Co (Publishers) Ltd., London, 1973.

28. S. P. Timoshenko, *History of Strength of Materials*, McGraw-Hill Book Company, New York, 1953.

29. R. W. Clough, "The Finite Element in Plane Stress Analysis", *Proceedings*, 2nd ASCE Conference on Electronic Computation, Pittsburgh, Pa., Sept. 1960.

30. M. J. Turner, R. W. Clough, H. C. Martin, and L. J. Topp, "Stiffness and Deflection Analysis of Complex Structures", *Journal of Aeronautical Sciences* Vol. 23, No. 9, pp. 805-823, 1956.

31. J. H. Argyris, and S. Kelsey, *Energy Theorems and Structural Analysis* (Collection of papers published in *Aircraft Engineering* in 1954 and 1955), Butterworths Scientific Publications, London, 1960.

32. R. J. Melosh, "Basis for Derivation of Matrices for the Direct Stiffness Method", *Journal American Institute for Aeronautics and astronautics* Vol. 1, pp. 1631-37, 1965.

33. O. C. Zienkiewicz, Y. K. Cheung, *The Finite Element Method in Engineering Science* : 2nd Edition, McGraw-Hill Book Company, London, 1971.

34. W. Visser, "A Finite Element Method for the Determination of Non-Stationary Temperature Distribution and Thermal Deformations", *Proceedings Conference on Matrix Methods in Structural Mechanics*, Air Force Institute of Technology, Wright Patterson Air Force Base, Dayton, Ohio, 1965.

35. Edward L. Wilson, and Robert E. Nickell, "Application of the Finite Element Method to Heat Conduction Analysis", *Nuclear Engineering and Design* Vol. 4, pp. 276-286, 1966.

36. Barna A. Szabo, and George C. Lee, "Derivation of Stiffness Matrices for Problems in Plane Elasticity by Galerkin's Method", *International Journal of Numerical Methods in Engineering* Vol. 1, pp. 301-310, 1969.

37. J. T. Oden, *Finite Elements of Nonlinear Continua*, McGraw-Hill Book Company, New York, 1972.

38. O. L. Roufaeil, "A New Four-Node Quadrilateral Plate Bending Element", *Journal of Computers & Structures* Vol. 54, No. 5, pp. 871-879, Great Britain, 1995.

39. Robert D. Cook, *Finite Element Modelling for Stress Analysis*, John Wiley & Sons, Inc, U.S.A, 1994.

40. James F. Shackelford, William Alexander, and Jun S. Park, *Materials Science and Engineering Handbook* : 2nd Edition, CRC Press, U.S.A, 1994.